Advances in Nano Research, *Vol. 12, No. 2 (2022) 117-137*
https://doi.org/10.12989/anr.2022.12.2.117

Novel quasi 3D theory for mechanical responses of FG-CNTs reinforced composite nanoplates

Mashhour A. Alazwari[1a], Ahmed Amine Daikh[2b] and Mohamed A. Eltaher*[1,3]

[1]*Faculty of Engineering, Mechanical Engineering Department, King Abdulaziz University, P.O. Box 80204, Jeddah, Saudi Arabia*
[2]*Department of Technology, University Centre of Naama, 45000 Naama, P.O. Box 66, Algeria*
[3]*Faculty of Engineering, Mechanical Design and Production Department, Zagazig University, P.O. Box 44519, Zagazig, Egypt*

(*Received June 12, 2021, Revised November 6, 2021, Accepted November 8, 2021*)

Abstract. Effect of thickness stretching on free vibration, bending and buckling behavior of carbon nanotubes reinforced composite (CNTRC) laminated nanoplates rested on new variable elastic foundation is investigated in this paper using a developed four-unknown quasi-3D higher-order shear deformation theory (HSDT). The key feature of this theoretical formulation is that, in addition to considering the thickness stretching effect, the number of unknowns of the displacement field is reduced to four, and which is more than five in the other models. Two new forms of CNTs reinforcement distribution are proposed and analyzed based on cosine functions. By considering the higher-order nonlocal strain gradient theory, microstructure and length scale influences are included. Variational method is developed to derive the governing equation and Galerkin method is employed to derive an analytical solution of governing equilibrium equations. Two-dimensional variable Winkler elastic foundation is suggested in this study for the first time. A parametric study is executed to determine the impact of the reinforcement patterns, nonlocal parameter, length scale parameter, side-t-thickness ratio and aspect ratio, elastic foundation and various boundary conditions on bending, buckling and free vibration responses of the CNTRC plate.
Keywords: critical buckling load; frequencies; Galerkin method; nonlocal strain gradient theory; quasi 3D HSDT; stresses and deflection; 2D Winkler elastic foundation

1. Introduction

The exceptional mechanical, thermal and electrical properties of carbon nanotubes (CNTs) have attracted increasing attention in recent years, Eltaher (2016, 2018). CNTs can be effectively dispersed or introduced in fine structures (for example, foams, films, polymer fibers, etc.) as compared to conventional fillers, Grag *et al*. (2021). Functionally graded materials (FGMs), whose composition designed to change continuously through a certain spatial direction (Akbaş *et al*. 2020), are employed in micro/nano-electro-mechanical system (MEMS/NEMS) and atomic force microscopes (AFMs) to achieve high sensitivity and desired performance, Abo-Bakr *et al*. (2020). This proper combination of CNTs and FGM concept was first introduced by Shen (2009) studying the nonlinear bending behavior of functionally graded carbon nanotube reinforced composites (FG-CNTRC) plates. Vibration and stability problems of the nanostructures such as nano beams and nanorods were investigated in detail by Yayli (2015a, b, 2016, 2018a, b, c, 2019).

Shojaee *et al*. (2017) used the transformed differential quadrature method to study the vibration of FG-CNTRC cylindrical panels. Gholami and Ansari (2018) studied the influence of geometrical imperfection on the nonlinear resonance of FG-CNTRC rectangular plates under a harmonic excitation transverse load. Alibeigloo (2018) exploited Fourier series expansion and generalized coupled thermoelectricity in predicting the transient response of a simply supported FG-CNTRC plate with a different pattern of CNT distribution and under thermal shock. Karami *et al*. (2018) exploited second order shear deformation theory to study critical buckling of FG-CNTRC plates rested on Winkler–Pasternak elastic foundation. Li *et al*. (2019) used Halpin–Tsai micromechanics model to evaluate mechanical properties of graphene nanoplatelet (GPL) reinforced nano-composite beams and studied primary and secondary resonances of these nanostructures. Selim *et al*. (2019) studied active vibration control of FG-GPL plates integrated with piezoelectric layers by using the element-free improved moving least-squares Ritz and higher-order shear deformation theory. Qaderi and Ebrahimi (2020) studied a vibration of polymer composite plates reinforced with graphene platelets resting on two-parameter viscoelastic foundation by using Halpin–Tsai homogenization procedure. Hussain *et al*. (2020a, b) analyzed the orthotropic vibration frequencies of CNTs with different orientations and boundary conditions. Ghassabi *et al*. (2020) studied the vibro-acoustic performance of CNTRC doubly curved 3D thick shells. Shakouri and Mohseni (2020) evaluated the critical buckling load of FG-GPLs sandwich plates using the first order shear theory. Amiri *et al*. (2020) studied the stress and buckling behaviors of micro-cylindrical sandwich panel reinforced by CNTs/GPL composite based on the higher order shear deformation theory and modified couple

*Corresponding author, Professor,
E-mail: meltaher@kau.edu.sa
[a] Ph.D., E-mail: maalazwari@kau.edu.sa
[b] Ph.D., E-mail: ahmed.amine.daikh@gmail.com

ISSN: 2287-237X (Print), 2287-2388 (Online)

stress theory. Sari *et al*. (2020) examined the buckling response of FG-GPL under combined thermal and mechanical loadings by using nonlocal elasticity. Daikh *et al*. (2021b) developed a broad analysis to study the static buckling and deflection of axially FG-CNTRC plates with temperature dependent material properties. Daikh *et al*. (2021c) studied the buckling response of curved FG-CNTRC nanobeam exposed to the thermal environment by using Galerkin method. Esen *et al*. (2021b, c) presented the dynamic response of FG-CNTRC and FG sigmoid nanobeam under moving point load by using nonlocal strain gradient theory.

Many researchers have been used the nonlocal strain gradient theory to incorporate the length scale and microstructure effects on the mechanical responses of nanostructures. Ghorbanpour *et al*. (2018) examined the size-dependent buckling response of nanoplate integrated with magnetoelectroelastic layers by using a nonlocal theory and refined zigzag theory. Eltaher and Mohamed (2020) used doublet mechanics theory in nonlinear buckling and vibration analyses of imperfect CNTs model as Euler-Bernoulli beam structures. Daikh *et al*. (2020a) studied static analysis of multilayer nonlocal strain gradient FG-CNTs nanobeam in the frame of higher shear deformation beam theory with hyperbolic function. Kolahdouzan *et al*. (2020) investigated vibration and buckling of FG-CNTRC sandwich annular nanoplates elastically restrained. Abdelrahman *et al*. (2021) studied the dynamic response of perforated nanobeams under moving mass by using the finite element method. Arshid *et al*. (2021) exploited modified couple stress theory to study the buckling stability of FG porous sandwich curved microbeams under thermal and magnetic fields. Eltaher *et al*. (2021) studied the size-dependent dynamic response of Timoshenko CNTs under moving load by using doublet mechanics. Esen *et al*. (2021a) studied analytically the vibration and buckling of FG nanobeam under the thermal and magnetic fields by using power-law distribution and Timoshenko beam theory. Thai *et al*. (2021) used nonlocal strain gradient meshfree plate approach to investigate the bending and vibration behavior of laminated and sandwich nanoplates in the frame of higher order shear deformation theory. Singh and Azam (2021) investigated the vibration of FG nanoplate embedded in hygrothermal environment by using Rayleigh-Ritz method.

To include the influence of shear on the mechanical behavior of classical/nonclassical nanostructures, many theories such as first order shear deformation theory, Reddy higher order shear theory (RHOSDT), Levinson theory, Quasi 3D theory, and zigzag layer-wise theory are proposed, (Bensaid 2017, Bekhadda *et al*. 2019, Belarbi *et al*. 2020). Ebrahimi and Barati (2016) developed an analytical solution for nonlocal buckling characteristics of higher-order inhomogeneous nanobeams embedded in an elastic medium. Eltaher *et al*. (2016b) illustrated the static stability of nonlocal nanobeams by using higher-order beam theories. Bouazza *et al*. (2017) investigated the free vibration of composite plates are by using a refined simple nth-higher-order shear deformation theory. Ehyaei *et al*. (2017) presented the influence of porosity and axial preload on the vibration behavior of rotating FG nanobeam. Abualnour *et al*. (2018) exploited a quasi-3D trigonometric plate theory to analyze the free vibration of composite plates. Zaoui *et al*. (2019) exploited new 2D and quasi-3D shear deformation theories in analyzing the free vibration of FG plates rested on an elastic foundation. Melaibari *et al*. (2020) and Hamed *et al*. (2020) studied the buckling behavior of FG and sandwich beam under variable axial load using higher order shear deformation theories. Based on the theory of elasticity, Shaban and Mazaheri (2020) presented the closed-form solution of bending of five-layer curved FG sandwich panel in magnetic field. Daikh *et al*. (2020c) and Daikh *et al*. (2021a, d) used new quasi 3D hyperbolic shear theory in conjoint with nonlocal strain gradient theory to study the bending, buckling and vibration behaviors of FG and FG-CNTRC sandwich nanoplates. Ghobadi *et al*. (2021) presented the effect of porosity distribution and electric field on stress and nonlinear vibration of FG nanoplates with the direct and inverse flexoelectric phenomenon. Alazwari *et al*. (2021) proposed a new HSDT for buckling of multilayered CNTs reinforced composite nanobeams supported on non-linear elastic foundations using various boundary conditions.

Li *et al*. (2021) examined natural frequencies of FGM plates rested on Winkler/Pasternak/Kerr foundation by using a simple quasi-3D HSDT. Sahmani *et al*. (2021) studied the nonlinear bending response of FG nanoplates with variable thickness including a surface elastic influence and shear effect developed by a quasi-3D plate model. Vinh and Huy (2021) illustrated the mechanical response of FG sandwich porous plate using a new hyperbolic shear deformation theory and finite element method. Zheng *et al*. (2021) used trigonometric four-variable shear deformation theory to analyze the buckling response of FG-GNPs reinforced composites sandwich microplates under a thermo-mechanical load. Daikh *et al*. (2021e) presented comprehensive analysis to investigate the buckling and deflection of axially FG-CNTRC plates with temperature-dependent material properties.

In the current study, the mechanical response of FG-CNTRC plates using simple and efficient formulations is analyzed. A new Quasi 3D HSDT is proposed to fulfil both parabolic shear distribution through the thickness and the zero-shear at free boundaries. Two new forms of CNTs reinforcement distribution are proposed and analyzed based on cosine functions. To cover the different boundary conditions, Galerkin method is used to develop a new analytical solution by considering the thickness stretching effect. The developed analytical model is then compared with other available theories in the literature. A new variable 2D Winkler elastic foundation is proposed in this work. The influence of CNTs reinforcement patterns, nonlocal parameter, length scale parameter, side-to-thickness ratio and aspect ratio, elastic foundation and various boundary conditions on the bending, buckling and free vibration responses of the CNTRC plate is examined in detail.

2. Problem statement

2.1 Material distribution functions

Consider a rectangular plate of length, width and thickness $a \times b \times h$. The plate is made of a polymer matrix and reinforced by CNTs. In addition to the uniform CNTs

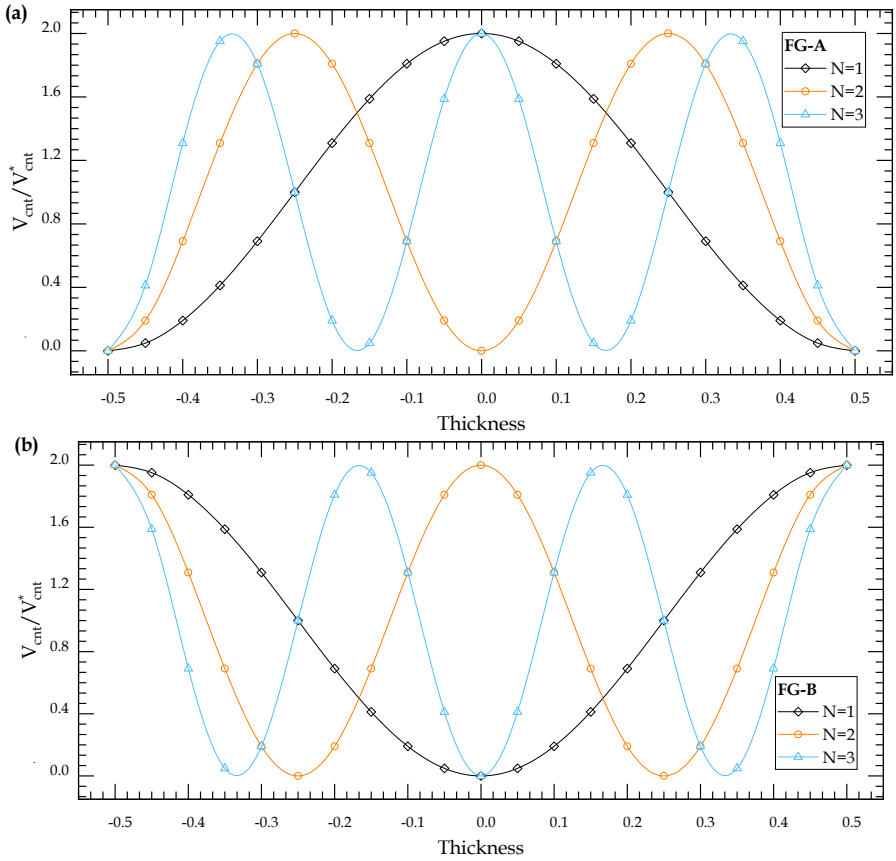

Fig. 1 Variation of CNTs volume fraction through th plate thickness

distribution, two new functionally graded distributions of CNTs reinforcement along the thickness of the plate are analysed in this work based on cosine function for the first time (as shown in Fig. 1).

The volume fraction of CNTs can be expressed as

Uniform distribution of CNTs (UD):

$$V_{cnt} = V^*_{cnt} \tag{1}$$

Functionally graded distribution of CNTs, type A (FG–A):

$$V_{cnt} = \left(1 + cos\left(N\frac{2\pi z}{h}\right)\right)V^*_{cnt} \; for \; N = 1,3,5 \ldots \tag{2}$$

$$V_{cnt} = \left(1 - cos\left(N\frac{2\pi z}{h}\right)\right)V^*_{cnt} \; for \; N = 2,4,6 \ldots \tag{3}$$

Functionally graded distribution of CNTs, type B (FG–B):

$$V_{cnt} = \left(1 + cos\left(N\frac{2\pi z}{h}\right)\right)V^*_{cnt} \; for \; N = 2,4,6 \ldots \tag{4}$$

$$V_{cnt} = \left(1 - cos\left(N\frac{2\pi z}{h}\right)\right)V^*_{cnt} \; for \; N = 1,3,5 \ldots \tag{5}$$

where N is the nonhomogeneity parameter, V^*_{cnt} is the total volume fraction of CNTs, which can be calculated as

$$V^*_{CNT} = \frac{W_{CNT}}{W_{cnt} + (\rho_{CNT}/\rho_m)(1 - W_{CNT})} \tag{6}$$

where W_{CNT} is the CNTs mass fraction, ρ_{CNT} is the CNTs mass density and ρ_m is polymer matrix mass density.

Young's modulus and shear modulus of the plate material is calculated employing the extended rule of the mixture and the molecular dynamics simulations and given by (Han and Elliott 2007)

$$E_{11} = \eta_1 V_{cnt} E^{cnt}_{11} + V_p E_p, \qquad \frac{\eta_2}{E_2} = \frac{V_{cnt}}{E^{cnt}_{22}} + \frac{V_p}{E_p}, \qquad \frac{\eta_3}{G_{12}} = \frac{V_{cnt}}{G^{cnt}_{12}} + \frac{V_p}{G_p} \tag{7}$$

E^k_{11} and E^k_{22} are Young's moduli in *x*-*y* directions, and G^k_{12} is the shear modulus. The subscripts p and cnt refer to the properties of the polymer and the CNTs. The parameters η_i $(i = 1,2,3)$ are the efficiency parameters of CNTs where $\eta_1 = 0.149$, $\eta_2 = \eta_3 = 0.934$, for the case of $V^*_{cnt} = 0.11$, $\eta_1 = 0.150$, $\eta_2 = \eta_3 = 0.941$, for the case of $V^*_{cnt} = 0.14$ and $\eta_1 = 0.149$, $\eta_2 = \eta_3 = 1.381$, for the case of $V^*_{cnt} = 0.17$ (Daikh *et al* 2020f).

The volume fraction of the polymer constituents V^k_p is related to CNTs volume fraction by:

$$V^k_{cnt} + V^k_p = 1 \tag{8}$$

Poisson's ratio ν_{12}, mass density ρ, thermal expansion coefficients in the longitudinal and transverse directions, α_{11} and α_{22} of k layer can be calculated by the relation (Shen 2009)

$$\nu_{12} = V_{cnt}\nu^{cnt}_{12} + V_p\nu_p \tag{9}$$

$$\rho = V_{cnt}\rho_{cnt} + V_p\rho_p \tag{10}$$

The other effective mechanical properties of a mixture

of the CNTs and the polymer are

$$E_{33}=E_{22},\quad G_{12}=G_{13}=G_{23},\quad \nu_{13}=\nu_{12},$$
$$\nu_{31}=\nu_{21},\quad \nu_{32}=\nu_{23}=\nu_{21},\quad \nu_{21}=\frac{E_{22}}{E_{11}}\nu_{12}$$

2.2 Nonlocal strain gradient theory

The nonlocal theory account for remote action forces between atoms. This causes the stresses to depend on the strains not only at an individual point under consideration but at all points of the body. The stresses generated by the defects in a nonlocally elastic medium have no non-physical singularities, in contrast to the corresponding solutions obtained in the classical theory of elasticity. Lim *et al*. (2015) proposed a function of stresses by including the strain gradient stress and nonlocal elastic stress fields which can be given as:

$$\sigma_{ij}=\sigma_{ij}^{(0)}-\frac{d\sigma_{ij}^{(1)}}{dx} \tag{11}$$

where $\sigma_{ij}^{(0)}$ and $\sigma_{ij}^{(1)}$ are the stresses corresponds to a strain ε_{kl} and strain gradient $\varepsilon_{kl,x}$, and can be written in the form

$$\begin{aligned}\sigma_{ij}^{(0)}&=\int_0^L C_{ijkl}\alpha_0(x,x',e_0a)\varepsilon_{kl,x}(x')dx'\\ \sigma_{ij}^{(1)}&=l^2\int_0^L C_{ijkl}\alpha_1(x,x',e_1a)\nabla\varepsilon_{kl,x}(x')dx'\end{aligned} \tag{12}$$

C_{ijkl} is the elastic constant, e_0a and e_1a are the nonlocal parameters and l is the strain gradient parameter. $\alpha_0(x,x',e_0a)$ and $\alpha_1(x,x',e_1a)$ are the nonlocal kernel functions (Eringen 1983). The constitutive relation of nonlocal strain gradient theory can be written as

$$\begin{aligned}&[1-(e_1a)^2\nabla^2][1-(e_0a)^2\nabla^2]\sigma_{ij}\\&=C_{ijkl}[1-(e_1a)^2\nabla^2]\varepsilon_{kl}-C_{ijkl}l^2[1-(e_0a)^2\nabla^2]\nabla^2\varepsilon_{kl}\end{aligned} \tag{13}$$

∇^2 indicates the Laplacian operator. By supposing that the coefficient $e=e_0=e_1$, The total constitutive relation can be expressed as, Lim *et al*. (2015)

$$[1-\mu\nabla^2]\sigma_{ij}=C_{ijkl}[1-\lambda\nabla^2]\varepsilon_{kl} \tag{14}$$

where $\mu=(ea)^2$ and $\lambda=l^2$.

2.3 Displacement field

The new proposed mathematical model is performed based on the classical plate theory (CPT) including the effect of transverse normal stress. The suggested formulations have four variables, which is even less than the other quasi-3D theories with five or more variable's displacement. Therefore, the displacement field can be expressed as:

$$\begin{aligned}u(x,y,z,t)&=u_0-z\frac{\partial w_0}{\partial x}-\beta\mathrm{f}(z)\frac{\partial^3 w_0}{\partial x^3}\\ v(x,y,z,t)&=v_0-z\frac{\partial w_0}{\partial y}-\beta\mathrm{f}(z)\frac{\partial^3 w_0}{\partial y^3}\\ w(x,y,z,t)&=w_0+\beta\frac{\mathrm{df}(z)}{\mathrm{d}z}\psi_z\end{aligned} \tag{15}$$

where, u_0, v_0, and w_0 are the horizontal and vertical displacement at the midplane of the plate. The additional displacement ψ_z accounts for the transverse normal stress effect. the shape function $\mathrm{f}(z)$ represents $\mathrm{f}(z)$ is a shape function that represents the distribution of the transverse shear strains and shear stresses. In the present analysis, a novel hyperbolic sine function shear deformation theory has been proposed as

$$\mathrm{f}(z)=h\sinh\left(\frac{z}{h}\right)-\frac{3z^3}{2h^2} \tag{16}$$

Based on the displacement field relations given in Eq. (15), the nonzero strains can be evaluated by

$$\begin{aligned}\begin{Bmatrix}\varepsilon_{xx}\\ \varepsilon_{yy}\\ \gamma_{xy}\end{Bmatrix}&=\begin{bmatrix}\varepsilon_{xx}^{(0)} & \varepsilon_{xx}^{(1)} & \varepsilon_{xx}^{(2)}\\ \varepsilon_{yy}^{(0)} & \varepsilon_{yy}^{(1)} & \varepsilon_{yy}^{(2)}\\ \gamma_{xy}^{(0)} & \gamma_{xy}^{(1)} & \gamma_{xy}^{(2)}\end{bmatrix}\begin{Bmatrix}1\\ \mathrm{z}\\ \mathrm{f}(z)\end{Bmatrix}\\ \begin{Bmatrix}\gamma_{yz}\\ \gamma_{xz}\end{Bmatrix}&=\beta\mathrm{f}'(z)\begin{Bmatrix}\gamma_{yz}^0\\ \gamma_{xz}^0\end{Bmatrix}\\ \varepsilon_{zz}&=\beta\mathrm{f}''(z)\varepsilon_{zz}^0\end{aligned} \tag{17}$$

where

$$\begin{Bmatrix}\varepsilon_{xx}^{(0)}\\ \varepsilon_{yy}^{(0)}\\ \gamma_{xy}^{(0)}\end{Bmatrix}=\begin{Bmatrix}\frac{\partial u_0}{\partial x}\\ \frac{\partial v_0}{\partial y}\\ \frac{\partial v_0}{\partial x}+\frac{\partial u_0}{\partial y}\end{Bmatrix},\quad \begin{Bmatrix}\varepsilon_{xx}^{(1)}\\ \varepsilon_{yy}^{(1)}\\ \gamma_{xy}^{(1)}\end{Bmatrix}=-\begin{Bmatrix}\frac{\partial^2 w_0}{\partial x^2}\\ \frac{\partial^2 w_0}{\partial y^2}\\ 2\frac{\partial^2 w_0}{\partial x\partial y}\end{Bmatrix},$$
$$\begin{Bmatrix}\varepsilon_{xx}^{(2)}\\ \varepsilon_{yy}^{(2)}\\ \gamma_{xy}^{(2)}\end{Bmatrix}=-\begin{Bmatrix}\frac{\partial^4 w_0}{\partial x^4}\\ \frac{\partial^4 w_0}{\partial y^4}\\ \frac{\partial(\nabla^2 w_0)}{\partial x\partial y}\end{Bmatrix},\quad \begin{Bmatrix}\gamma_{xz}^{(0)}\\ \gamma_{yz}^{(0)}\end{Bmatrix}=\begin{Bmatrix}-\frac{\partial^3 w_0}{\partial x^3}+\frac{\partial\psi_z}{\partial x}\\ -\frac{\partial^3 w_0}{\partial y^3}+\frac{\partial\psi_z}{\partial y}\end{Bmatrix}, \tag{18}$$
$$\varepsilon_{zz}^{(0)}=\psi_z,\ \nabla^2 w_0=\frac{\partial^2 w_0}{\partial x^2}+\frac{\partial^2 w_0}{\partial y^2}$$

Then, the constitutive stress-strain relations of can be stated as

$$\begin{aligned}&[1-\mu\nabla^2]\begin{Bmatrix}\sigma_{xx}\\ \sigma_{yy}\\ \sigma_{zz}\\ \tau_{yz}\\ \tau_{xz}\\ \tau_{xy}\end{Bmatrix}\\&=[1-\lambda\nabla^2]\begin{bmatrix}Q_{11} & Q_{12} & Q_{13} & 0 & 0 & 0\\ Q_{12} & Q_{22} & Q_{23} & 0 & 0 & 0\\ Q_{13} & Q_{23} & Q_{33} & 0 & 0 & 0\\ 0 & 0 & 0 & Q_{44} & 0 & 0\\ 0 & 0 & 0 & 0 & Q_{55} & 0\\ 0 & 0 & 0 & 0 & 0 & Q_{66}\end{bmatrix}\begin{Bmatrix}\varepsilon_{xx}\\ \varepsilon_{yy}\\ \varepsilon_{zz}\\ \gamma_{yz}\\ \gamma_{xz}\\ \gamma_{xy}\end{Bmatrix}\end{aligned} \tag{19}$$

In which

$$\begin{aligned}&Q_{11}=\frac{E_{11}}{\Delta}(1-\nu_{23}\nu_{32}),\qquad Q_{22}=\frac{E_{22}}{\Delta}(1-\nu_{31}\nu_{13}),\\&Q_{33}=\frac{E_{33}}{\Delta}(1-\nu_{12}\nu_{21}),\qquad Q_{44}=G_{23},\\&Q_{55}=G_{13},\ Q_{66}=G_{12},\ Q_{12}=\tfrac{E_{11}}{\Delta}(\nu_{21}+\nu_{31}\nu_{23}),\\&Q_{13}=\frac{E_{11}}{\Delta}(\nu_{31}+\nu_{21}\nu_{32}),\qquad Q_{23}=\frac{E_{22}}{\Delta}(\nu_{32}+\nu_{12}\nu_{31})\\&\Delta=1-\nu_{12}\nu_{21}-\nu_{23}\nu_{32}-\nu_{31}\nu_{13}-2\nu_{12}\nu_{32}\nu_{13}\end{aligned} \tag{20}$$

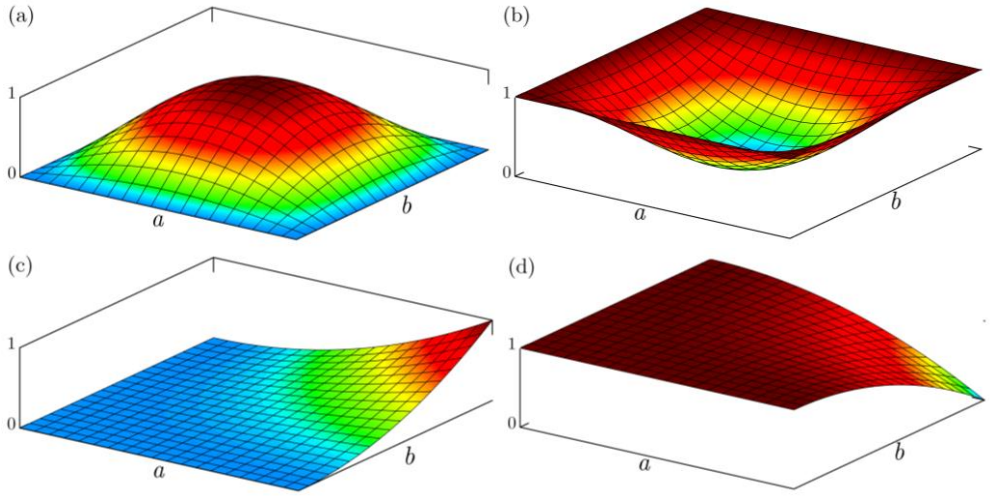

Fig. 2 Winkler elastic foundation intensity $(\kappa = 0, \xi = 1)$; (a): Sinusoidal, (b): Reverse sinusoidal, (c): Parabolic, (d): Reverse parabolic.

2.4 Variational statements

Utilizing the principle of Hamilton, the equations of motion of the CNTRC nanoplate can be derived as:

$$\delta \int_{t_2}^{t_1} \delta(U - T + V)dt = 0 \tag{21}$$

Here, U, T and V are the strain energy, the kinetic energy and the virtual work done by external forces, respectively.

The virtual strain energy of the plate can be written as

$$\delta U = \int_V {\sigma_{ij}}^{(n)} \delta \varepsilon_{ij} \mathrm{d}V \tag{22}$$

$$\int_\Omega \int \begin{bmatrix} N_{xx}\frac{\partial \delta u_0}{\partial x} - M_{xx}\frac{\partial^2 \delta w_0}{\partial x^2} - \beta S_{xx}\frac{\partial^4 \delta w_0}{\partial x^4} \\ +N_{yy}\frac{\partial \delta v_0}{\partial y} - M_{yy}\frac{\partial^2 \delta w_0}{\partial y^2} - \beta S_{yy}\frac{\partial^4 \delta w_0}{\partial y^4} \\ +\beta Q_{zz}\delta\psi_z + N_{xy}\left(\frac{\partial \delta u_0}{\partial y} + \frac{\partial \delta v_0}{\partial x}\right) - 2M_{xy}\frac{\partial^2 \delta w_0}{\partial x \partial y} \\ -\beta S_{xy}\left(\frac{\partial^4 \delta w_0}{\partial x^3 \partial y} + \frac{\partial^4 \delta w_0}{\partial x \partial y^3}\right) + \beta R_{yz}\frac{\partial \delta \psi_z}{\partial y} \\ -\beta R_{yz}\frac{\partial^3 \delta w_0}{\partial y^3} + +\beta R_{xz}\frac{\partial \delta \psi_z}{\partial x} - R_{xz}\frac{\partial^3 \delta w_0}{\partial x^3} \end{bmatrix} \mathrm{d}x\mathrm{d}y\mathrm{d}z \tag{23}$$

In which the force and moment resultants are defined by:

$$\begin{aligned} \{N_{ij}, M_{ij}, S_{ij}\} &= \int_{-h/2}^{h/2} \{1, z, \Phi(z)\}\sigma_{ij}\mathrm{d}z, \quad i,j = x,y \\ R_{iz} &= \int_{-h/2}^{h/2} \Phi'(z)\,\sigma_{iz}\mathrm{d}z, \; Q_{zz} = \int_{-h/2}^{h/2} \Phi''(z)\,\sigma_{zz}\mathrm{d}z \end{aligned} \tag{24}$$

By including the effect of in-plane compressive loads $\bar{N}^0_{xx} = \chi_1 N_{cr}$ and $\bar{N}^0_{yy} = \chi_2 N_{cr}$, where χ_1 and χ_2 are the buckling loading intensity, transverse load q and the variable Winkler elastic foundation f_e, the virtual work can be stated as

$$\delta V = -\int_A (q - f_e)\delta w \mathrm{d}A \tag{25}$$

$$+\int_A \left[\bar{N}^0_{xx}\frac{\partial w_0}{\partial x}\frac{\partial \delta w_0}{\partial x} + \bar{N}^0_{yy}\frac{\partial w_0}{\partial y}\frac{\partial \delta w_0}{\partial y}\right]\mathrm{d}A \tag{25}$$

where

$$f_e = k_w(w_0 + f'(z)\psi_z) \tag{26}$$

where k_w denote the modulus of subgrade reaction (elastic coefficient of Winkler foundation). The proposed Winkler foundation varies through *x* and *y* directions based on two parameters κ and ξ:

$$k_w = \kappa + \xi \begin{cases} \sin\left(\frac{\pi x}{a}\right)\sin\left(\frac{\pi y}{b}\right) & \text{Sinusoidal} \\ 1 - \sin\left(\frac{\pi x}{a}\right)\sin\left(\frac{\pi y}{b}\right) & \text{Reverse Sinusoidal} \\ \left(\frac{xy}{ab}\right)^2 & \text{Parabolic} \\ 1 - \left(\frac{xy}{ab}\right)^2 & \text{Reverse Parabolic} \end{cases} \tag{27}$$

The variation kinetic energy can be expressed as:

$$\delta K = \int_V [\dot{u}\delta\dot{u} + \dot{v}\delta\dot{v} + \dot{w}\delta\dot{w}]\mathrm{d}x\mathrm{d}y\mathrm{d}z \tag{28}$$

$$\begin{aligned} &= \int_V \left\{ \begin{array}{c} I_0(\dot{u}_0\delta\dot{u}_0 + \dot{v}_0\delta\dot{v}_0 + \dot{w}_0\delta\dot{w}_0) \\ -I_1\left(\frac{\partial \dot{w}_0}{\partial x}\delta\dot{u}_0 + \frac{\partial \dot{w}_0}{\partial y}\delta\dot{v}_0 + \dot{u}_0\frac{\partial \delta\dot{w}_0}{\partial x} + \dot{v}_0\frac{\partial \delta\dot{w}_0}{\partial y}\right) \\ +\beta I_3\left(\begin{array}{c} \dot{u}_0\frac{\partial^3 \delta\dot{w}_0}{\partial x^3} + \frac{\partial^3 \dot{w}_0}{\partial x^3}\delta\dot{u}_0 \\ +\dot{v}_0\frac{\partial^3 \delta\dot{w}_0}{\partial y^3} + \frac{\partial^3 \dot{w}_0}{\partial y^3}\delta\dot{v}_0 \end{array}\right) + I_2\left(\begin{array}{c} \frac{\partial \dot{w}_0}{\partial x}\frac{\partial \delta\dot{w}_0}{\partial x} \\ +\frac{\partial \dot{w}_0}{\partial y}\frac{\partial \delta\dot{w}_0}{\partial y} \end{array}\right) \\ +\beta^2 I_4\left(\begin{array}{c} \frac{\partial \dot{w}_0}{\partial x}\frac{\partial^3 \delta\dot{w}_0}{\partial x^3} + \frac{\partial^3 \dot{w}_0}{\partial x^3}\frac{\partial \delta\dot{w}_0}{\partial x} \\ +\frac{\partial \dot{w}_0}{\partial y}\frac{\partial^3 \delta\dot{w}_0}{\partial y^3} + \frac{\partial^3 \dot{w}_0}{\partial y^3}\frac{\partial \delta\dot{w}_0}{\partial y} \end{array}\right) \\ +\beta^2 I_5\left(\frac{\partial^3 \dot{w}_0}{\partial x^3}\frac{\partial^3 \delta\dot{w}_0}{\partial x^3} + \frac{\partial^3 \dot{w}_0}{\partial y^3}\frac{\partial^3 \delta\dot{w}_0}{\partial y^3}\right) \\ +\beta J_0(\dot{\varphi}_z\delta\dot{w}_0 + \dot{w}_0\delta\dot{\varphi}_z) + \beta^2 J_1(\dot{\varphi}_z\delta\dot{\varphi}_z) \end{array} \right\} \mathrm{d}x\mathrm{d}y\mathrm{d}z \end{aligned} \tag{29}$$

In which

$$\{I_0, I_1, I_2, I_3, I_4, I_5\} = \int_{-h/2}^{h/2} \rho(z)\left\{1, z, z^2, \mathrm{f}(z), z\mathrm{f}(z), \left(\mathrm{f}(z)\right)^2\right\}\mathrm{d}z$$
$$\{J_0, J_1\} = \int_{-h/2}^{h/2} \rho(z)\left\{\mathrm{g}(z), \left(\mathrm{g}(z)\right)^2\right\}\mathrm{d}z \tag{30}$$

Thence, the equations of motion of the CNTRC plate can be described by

$$\begin{aligned}
\delta u_0 &: \frac{\partial N_{xx}}{\partial x} + \frac{\partial N_{xy}}{\partial y} = I_0\ddot{u}_0 - I_1\frac{\partial \ddot{w}_0}{\partial x} - I_3\beta\frac{\partial^3 \ddot{w}_0}{\partial x^3}\\
\delta v_0 &: \frac{\partial N_{xy}}{\partial x} + \frac{\partial N_{yy}}{\partial y} = I_0\ddot{v}_0 - I_1\frac{\partial \ddot{w}_0}{\partial y} - I_3\beta\frac{\partial^3 \ddot{w}_0}{\partial y^3}\\
\delta w_0 &: \frac{\partial^2 M_{xx}}{\partial x^2} + 2\frac{\partial^2 M_{xy}}{\partial x\partial y} + \frac{\partial^2 M_{yy}}{\partial y^2} + \beta\left(\frac{\partial^4 S_{xx}}{\partial x^4} + \frac{\partial^4 S_{xx}}{\partial y^4} + \frac{\partial^4 S_{xy}}{\partial x^3\partial y} + \frac{\partial^4 S_{xy}}{\partial x\partial y^3} - \frac{\partial^3 R_{yz}}{\partial y^3} - \frac{\partial^3 R_{xz}}{\partial x^3}\right)\\
&\quad + q - f_e + \bar{N}^0_{xx}\frac{\partial^2 w_0}{\partial x^2} + \bar{N}^0_{yy}\frac{\partial^2 w_0}{\partial y^2}\\
&= I_0\ddot{w}_0 + I_1\left(\frac{\partial \ddot{u}_0}{\partial x} + \frac{\partial \ddot{v}_0}{\partial y}\right) - I_2\left(\frac{\partial^2 \ddot{w}_0}{\partial x^2} + \frac{\partial^2 \ddot{w}_0}{\partial y^2}\right) + \beta I_3\left(\frac{\partial^3 \ddot{u}_0}{\partial x^3} + \frac{\partial^3 v}{\partial y^3}\right)\\
&\quad - 2\beta I_4\left(\frac{\partial^4 \ddot{w}_0}{\partial x^4} + \frac{\partial^4 \ddot{w}_0}{\partial y^4}\right) - \beta^2 I_5\left(\frac{\partial^6 \ddot{w}_0}{\partial x^6} + \frac{\partial^6 \ddot{w}_0}{\partial y^6}\right) + \beta J_0\ddot{\psi}_z\\
\delta\psi_z &: \beta\left(\frac{\partial R_{xz}}{\partial x} + \frac{\partial R_{yz}}{\partial y} - Q_{zz} + \mathrm{g}(z)\left(q - f_e + \bar{N}^0_{xx}\frac{\partial^2 \ddot{\psi}_z}{\partial x^2} + \bar{N}^0_{yy}\frac{\partial^2 \ddot{\psi}_z}{\partial y^2}\right)\right) = \beta J_0\ddot{w}_0 + \beta^2 J_1\ddot{\psi}_z
\end{aligned} \tag{31}$$

Substituting of Eq. (31) into nonlocal strain gradient constitutive equation given by Eq. (19), yields

$$[1-\mu\nabla^2]\begin{Bmatrix} N_{xx}\\ N_{yy}\\ N_{xy}\\ M_{xx}\\ M_{yy}\\ M_{xy}\\ S_{xx}\\ S_{yy}\\ S_{xy}\\ Q_{zz}\end{Bmatrix} = [1-\lambda\nabla^2]\begin{bmatrix}
A_{11} & A_{12} & 0 & B_{11} & B_{12} & 0 & \beta C_{11} & \beta C_{12} & 0 & \beta G^a_{13}\\
A_{12} & A_{22} & 0 & B_{12} & B_{22} & 0 & \beta C_{12} & \beta C_{22} & 0 & \beta G^a_{13}\\
0 & 0 & A_{66} & 0 & 0 & B_{66} & 0 & 0 & \beta C_{66} & 0\\
B_{11} & B_{12} & 0 & D_{11} & D_{12} & 0 & \beta E_{11} & \beta E_{12} & 0 & \beta H^a_{13}\\
B_{12} & B_{22} & 0 & D_{12} & D_{22} & 0 & \beta E_{12} & \beta E_{22} & 0 & \beta H^a_{13}\\
0 & 0 & B_{66} & 0 & 0 & D_{66} & 0 & 0 & \beta E_{66} & 0\\
C_{11} & C_{12} & 0 & E_{11} & E_{12} & 0 & \beta H_{11} & \beta H_{12} & 0 & \beta J^a_{13}\\
C_{12} & C_{22} & 0 & E_{12} & E_{22} & 0 & \beta H_{12} & \beta H_{22} & 0 & \beta J^a_{13}\\
0 & 0 & C_{66} & 0 & 0 & E_{66} & 0 & 0 & \beta H_{66} & 0\\
\beta G^a_{13} & \beta G^a_{13} & 0 & \beta H^a_{13} & \beta H^a_{13} & 0 & \beta J^a_{13} & \beta J^a_{13} & 0 & \beta K^a_{13}
\end{bmatrix}\begin{Bmatrix} \varepsilon^{(0)}_{xx}\\ \varepsilon^{(0)}_{yy}\\ \gamma^{(0)}_{xy}\\ \varepsilon^{(1)}_{xx}\\ \varepsilon^{(1)}_{yy}\\ \gamma^{(1)}_{xy}\\ \varepsilon^{(2)}_{xx}\\ \varepsilon^{(2)}_{yy}\\ \gamma^{(2)}_{xy}\\ \psi_z\end{Bmatrix} \tag{32}$$

$$[1-\mu\nabla^2]\begin{Bmatrix} R_{xz}\\ R_{yz}\end{Bmatrix} = [1-\lambda\nabla^2]\begin{bmatrix} F_{55} & 0\\ 0 & F_{44}\end{bmatrix}\begin{Bmatrix}\gamma^{(0)}_{xz}\\ \gamma^{(0)}_{yz}\end{Bmatrix} \tag{33}$$

The stiffness coefficients can be written as

$$\begin{aligned}
\{A_{11}, B_{11}, C_{11}, D_{11}, E_{11}, H_{11}\} &= \int_{-h/2}^{h/2} \bar{Q}^k_{11}\left\{1, z, \mathrm{f}(z), z^2, z\mathrm{f}(z), \left(\mathrm{f}(z)\right)^2\right\}\mathrm{d}z\\
\{A_{12}, B_{12}, C_{12}, D_{12}, E_{12}, H_{12}\} &= \int_{-h/2}^{h/2} \bar{Q}^k_{12}\left\{1, z, \mathrm{f}(z), z^2, z\mathrm{f}(z), \left(\mathrm{f}(z)\right)^2\right\}\mathrm{d}z\\
\{A_{66}, B_{66}, C_{66}, D_{66}, E_{66}, H_{66}\} &= \int_{-h/2}^{h/2} \bar{Q}^k_{66}\left\{1, z, \mathrm{f}(z), z^2, z\mathrm{f}(z), \left(\mathrm{f}(z)\right)^2\right\}\mathrm{d}z
\end{aligned} \tag{34}$$

$$F_{44} = F_{55} = \int_{-h/2}^{h/2} \bar{Q}^k_{44}\left(\mathrm{f}'(z)\right)^2\mathrm{d}z, \qquad K^a_{33} = \int_{-h/2}^{h/2} \bar{Q}^k_{33}\left(\mathrm{f}''(z)\right)^2\mathrm{d}z, \qquad \{G^a_{13}, H^a_{13}, J^a_{13}\} = \int_{-h/2}^{h/2} \bar{Q}^k_{13}\{1, z, \mathrm{f}(z)\}\mathrm{f}''(z)\mathrm{d}z$$

The equation of motion in terms of displacements δu_0, δv_0, δw_0 and $\delta \varphi_z$ can be described by

$$(1-\lambda\nabla^2)\begin{bmatrix} A_{11}\frac{\partial^2 u_0}{\partial x^2}+A_{66}\frac{\partial^2 u_0}{\partial y^2}+(A_{12}+A_{66})\frac{\partial^2 v_0}{\partial x\partial y}-B_{11}\frac{\partial^3 w_0}{\partial x^3}-(B_{12}+2B_{66})\frac{\partial^3 w_0}{\partial x\partial y^2} \\ -\beta\left(C_{66}\frac{\partial^5 w_0}{\partial x^3\partial y^2}+(C_{12}+C_{66})\frac{\partial^5 w_0}{\partial x\partial y^4}+C_{11}\frac{\partial^5 w_0}{\partial x^5}\right)+G_{13}^a\frac{\partial \psi_z}{\partial x} \end{bmatrix} = (1-\mu\nabla^2)\left[I_0\frac{\partial^2 u_0}{\partial t^2}-I_1\frac{\partial^3 w_0}{\partial x\partial t^2}-\beta J_1\frac{\partial^5 w_0}{\partial x^3\partial t^2}\right] \tag{35}$$

$$(1-\lambda\nabla^2)\begin{bmatrix} A_{22}\frac{\partial^2 v_0}{\partial y^2}+A_{66}\frac{\partial^2 v_0}{\partial x^2}+(A_{12}+A_{66})\frac{\partial^2 u_0}{\partial x\partial y}-B_{22}\frac{\partial^3 w_0}{\partial y^3}-(B_{12}+2B_{66})\frac{\partial^3 w_0}{\partial x^2\partial y} \\ -\beta\left(C_{66}\frac{\partial^5 w_0}{\partial x^2\partial y^3}+(C_{12}+C_{66})\frac{\partial^5 w_0}{\partial x^4\partial x}+C_{22}\frac{\partial^5 w_0}{\partial y^5}\right)+G_{13}^a\frac{\partial \psi_z}{\partial y} \end{bmatrix} = (1-\mu\nabla^2)\left[I_0\frac{\partial^2 v_0}{\partial t^2}-I_1\frac{\partial^3 w_0}{\partial y\partial t^2}-\beta J_1\frac{\partial^5 w_0}{\partial y^3\partial t^2}\right] \tag{36}$$

$$(1-\lambda\nabla^2)\begin{bmatrix} B_{11}\frac{\partial^3 u_0}{\partial x^3}+(B_{12}+2B_{66})\frac{\partial^3 u_0}{\partial x\partial y^2}+(B_{12}+2B_{66})\frac{\partial^3 v_0}{\partial x^2\partial y}+B_{22}\frac{\partial^3 v_0}{\partial y^3} \\ -D_{11}\frac{\partial^4 w_0}{\partial x^4}-2(D_{12}+2D_{66})\frac{\partial^4 w_0}{\partial x^2\partial y^2}-D_{22}\frac{\partial^4 w_0}{\partial y^4}+\beta\left[C_{11}\frac{\partial^5 u_0}{\partial x^5}\right. \\ +(C_{12}+C_{66})\frac{\partial^5 u_0}{\partial x\partial y^4}+(C_{12}+C_{66})\frac{\partial^5 v_0}{\partial x^4\partial y}+C_{22}\frac{\partial^5 v_0}{\partial y^5}+C_{66}\frac{\partial^5 u_0}{\partial x^3\partial y^2} \\ +C_{66}\frac{\partial^5 v_0}{\partial x^2\partial y^3}-2E_{11}\frac{\partial^6 w_0}{\partial x^6}-2(E_{12}+2E_{66})\frac{\partial^6 w_0}{\partial x^2\partial y^4} \\ \left.-2(E_{12}+2E_{66})\frac{\partial^6 w_0}{\partial x^4\partial y^2}-2E_{22}\frac{\partial^6 w_0}{\partial y^6}\right]-\beta^2\left[H_{11}\frac{\partial^8 w_0}{\partial x^8}+2(H_{12}+H_{66})\frac{\partial^8 w_0}{\partial x^4\partial y^4}\right. \\ +H_{66}\frac{\partial^8 w_0}{\partial x^6\partial y^2}+H_{66}\frac{\partial^8 w_0}{\partial x^2\partial y^6}+H_{22}\frac{\partial^8 w_0}{\partial y^8}-F_{44}\frac{\partial^6 w_0}{\partial x^6}-F_{55}\frac{\partial^6 w_0}{\partial y^6}\Big] \\ \left.+\beta J_{13}^a\left(\frac{\partial^4 \psi_z}{\partial x^4}+\frac{\partial^4 \psi_z}{\partial y^4}\right)+G_{13}^a\left(\frac{\partial^2 \psi_z}{\partial x^2}+\frac{\partial^2 \psi_z}{\partial y^2}\right)-F_{44}\frac{\partial^4 \psi_z}{\partial y^4}-F_{55}\frac{\partial^4 \psi_z}{\partial x^4}\right] \\ +(1-\mu\nabla^2)\left[q-f_e+\bar{N}_{xx}^0\frac{\partial^2 w_0}{\partial x^2}+\bar{N}_{yy}^0\frac{\partial^2 w_0}{\partial y^2}\right] \\ = (1-\mu\nabla^2)\left[I_0\frac{\partial^2 w_0}{\partial t^2}+I_1\left(\frac{\partial^3 u_0}{\partial x\partial t^2}+\frac{\partial^3 v_0}{\partial y\partial t^2}\right)+\beta I_3\left(\frac{\partial^5 u_0}{\partial x^3\partial t^2}+\frac{\partial^5 v_0}{\partial y^3\partial t^2}\right)\right. \\ \left.-I_2\left(\frac{\partial^4 w_0}{\partial x^2\partial t^2}+\frac{\partial^4 w_0}{\partial y^2\partial t^2}\right)-2\beta I_4\left(\frac{\partial^6 w_0}{\partial x^4\partial t^2}+\frac{\partial^6 w_0}{\partial y^4\partial t^2}\right)-\beta^2 I_5\left(\frac{\partial^8 w_0}{\partial x^6\partial t^2}+\frac{\partial^8 w_0}{\partial y^6\partial t^2}\right)+J_0\frac{\partial^2 \psi_z}{\partial t^2}\right] \tag{37}$$

$$(1-\lambda\nabla^2)\begin{bmatrix} -\beta G_{13}^a\left(\frac{\partial u_0}{\partial x}+\frac{\partial v_0}{\partial y}\right)+\beta H_{13}^a\left(\frac{\partial^2 w_0}{\partial x^2}+\frac{\partial^2 w_0}{\partial y^2}\right)+\beta^2(J_{13}^a-F_{55})\frac{\partial^4 w_0}{\partial x^4} \\ +\beta^2(J_{13}^a-F_{44})\frac{\partial^4 w_0}{\partial y^4}+\beta^2\left(F_{55}\frac{\partial^2 \psi_z}{\partial x^2}+F_{44}\frac{\partial^2 \psi_z}{\partial y^2}-K_{33}^a\psi_z\right) \end{bmatrix} \\ +(1-\mu\nabla^2)\left[\beta g(z)\left(q-f_e+\bar{N}_{xx}^0\frac{\partial^2 \ddot{\psi}_z}{\partial x^2}+\bar{N}_{yy}^0\frac{\partial^2 \ddot{\psi}_z}{\partial y^2}\right)\right] \\ = (1-\mu\nabla^2)\left[J_0\frac{\partial^2 w_0}{\partial t^2}+J_1\frac{\partial^2 \psi_z}{\partial t^2}\right] \tag{38}$$

3. Analytical solution

In this, we develop an analytical solution of Eqs. (35)-(38) using Galerkin method by considering different boundary conditions. The generalized displacements can be written as:

Table 1 Material properties of SWCNT (10, 10)

$T[K]$	E_{11}^{cnt}[TPa]	E_{22}^{cnt}[TPa]	G_{12}^{cnt}[TPa]	ν_{11}^{cnt}	$\alpha_{11}^{cnt}[10^{-6}/K]$	$\alpha_{22}^{cnt}[10^{-6}/K]$
300	5.6466	7.0800	1.9445	0.175	3.4584	5.1682
400	5.5679	6.9814	1.9703	0.175	4.1496	5.0905
500	5.5308	6.9348	1.9643	0.175	4.5361	5.0189
700	5.4744	6.8641	1.9644	0.175	4.6677	4.8943

Table 2 Temperature-dependent coefficients of CNTs material properties

	P_0	P_{-1}	P_1	P_2	P_3
E_{11}^{cnt}[TPa]	6.3998	0	-6.77898×1e-4	1.16097×1e-6	-6.96636×1e-10
E_{22}^{cnt}[TPa]	8.02155	0	-6.75726×1e-4	1.15626×1e-6	-6.93444×1e-10
G_{12}^{cnt}[TPa]	1.40755	0	2.46968×1e-3	-4.94831×1e-6	3.18224×1e-9
$\alpha_{11}[10^{-6}/°C]$	-1.12515	0	-2.03678×1e-2	2.56588×1e-5	-1.00986×1e-8
$\alpha_{22}[10^{-6}/°C]$	5.43715	0	-1.81092×1e-4	5.33367×1e-8	2.29899×1e-12
ν_{12}^{cnt}	0.175	0	0	0	0

$$u_0 = \sum_{m=1}^{\infty}\sum_{n=1}^{\infty} U_{mn}\frac{\partial X_m(x)}{\partial x}Y_n(y)e^{i\omega t}$$
$$v_0 = \sum_{m=1}^{\infty}\sum_{n=1}^{\infty} V_{mn}X_m(x)\frac{\partial Y_n(y)}{\partial y}e^{i\omega t} \quad (39)$$
$$\{w_0, \psi_z\} = \sum_{m=1}^{\infty}\sum_{n=1}^{\infty}\{W_{mn}, \Psi_{mn}\}X_m(x)Y_n(y)\,e^{i\omega t}$$

where, U_{mn}, V_{mn}, W_{mn} and Ψ_{mn} are arbitrary parameters. m and n are the mode shape numbers. $X_m(x)$ and $Y_n(y)$ are the functions which satisfy the above boundary conditions and can be given as (Daikh *et al* 2021a):

$X_m(x) = \sin(\alpha x)$ and $Y_n(y) = \sin(\beta y)$, for the SSSS nanoplate.

$X_m(x) = \sin^2(\alpha x)$ and $Y_n(y) = \sin^2(\beta y)$, for the CCCC nanoplate.

$X_m(x) = \sin^2(\alpha x)$ and $Y_n(y) = \sin(\beta y)$, for the CCSS nanoplate.

$X_m(x) = \sin(\alpha x)[\cos(\alpha x) - 1]$ and $Y_n(y) = \sin(\beta y)[\cos(\beta y) - 1]$, for the CSCS nanoplate.

where $\lambda = m\pi/a$, $\mu = n\pi/b$. By substituting Eq. (39) in Eq. (35)-(38), one obtains

$$([\mathrm{K}]_{4\times4} - \omega^2[\mathrm{M}]_{4\times4})\begin{Bmatrix} U_{mn} \\ V_{mn} \\ W_{mn} \\ \psi_z \end{Bmatrix} = \begin{Bmatrix} 0 \\ 0 \\ q \\ 0 \\ 0 \end{Bmatrix} \quad (40)$$

where [K] and [M] are the rigidity matrix and mass matrix, respectively.

For the bending behaviour analysis, the applied sinusoidal load is given as (Thai *et al*. 2014):

$$q = -q_0\int_0^a\int_0^b \sin^2(\alpha x)\sin^2(\beta y)\,\mathrm{d}x\mathrm{d}y \quad (41)$$

4. Results and discussions

In this section, we analyse the mechanical response of three types of nanoplates made of a mixture of the polymer PmPV (matrix) and armchair (10, 10) single-walled CNTs (reinforcement). The plate is exposed to in-plane compressive loadings in the two directions $\left(\bar{N}_{xx}^0 = \chi_1 N_{cr}, \bar{N}_{yy}^0 = \chi_2 N_{cr}\right)$ for buckling analysis, and transverse sinusoidal loading for the bending analysis. Material properties of the polymer PmPV are temperature dependent and are given as (Shen 2009),

$$E_m = (3.51 - 0.0047\Delta T)\mathrm{GPa} \quad (42)$$

$$\alpha_m = 45(1 + 0.0005\Delta T)10^{-6}1/°K \quad (43)$$

Poisson ratio and the mass density are given as $\nu_m = 0.34$ and $\rho_m = 1150\,\mathrm{kg/m^3}$, respectively. Material properties of the CNTs constituent are stated in Table 1.

As we consider, the material properties of the nanoplate are dependent to the temperature. Employing Touloukian principal (Touloukian 1967, Daikh 2019, Daikh *et al.* 2020b), material properties can be written in the function of temperature as

$$P = P_0(P_{-1}T^{-1} + 1 + P_1T + P_2T^2 + P_3T^3) \quad (44)$$

where $T = T_0 + \Delta T$. T_0 is the ambient temperature $(T_0 = 300K)$, and ΔT is the difference between the temperature of the top surface and the bottom surface, and P_0, P_1, P_2, and P_3 are coefficients of temperature (see Table 2).

To simplify and standardize calculations, the dimensionless parameters for bending, buckling and vibration analyses of CNTRC plates are described using the following forms:

The dimensionless displacements:

$$\bar{w} = \frac{10^3 D_0}{a^4 q_0} w\left(\frac{a}{2}, \frac{b}{2}\right) \quad (45)$$

Table 3 Comparison of central deflection of simply supported square CNTRC plates for various kinds of CNTs distribution (a/h = 10, T = 300K, N = 1)

V_{cnt}^{*}	Theory	UD	FG X	FG O	FG V	FG–A	FG–B
0.11	Present	0.4965	0.4229	0.7081	0.5871	0.8081	0.4147
	TSDT(*)	0.4964	0.4227	0.7081	0.5869	-	-
	SSDT(*)	0.4953	0.4208	0.7104	0.5859	-	-
0.14	Present	0.4397	0.3819	0.6149	0.5134	0.7002	0.3760
	0.4396	0.3817	0.6148	0.5133	-	-	0.4396
	0.4383	0.3800	0.6168	0.5121	-	-	0.4383
0.17	0.3177	0.2725	0.4526	0.3770	0.5180	0.2675	0.3177
	0.3177	0.2723	0.4526	0.3769	-	-	0.3177
	0.3170	0.2715	0.4537	0.3763	-	-	0.3170

(*) Results obtained by Wattanasakulpong and Chaikittiratana (2013)

Table 4 Effect of temperature and CNTs volume fraction on the dimensionless deflection of simply supported square CNTRC plate (a/h = 10, T = 300K)

Temperature	N	$V_{cnt}^{*} = 0.11$			$V_{cnt}^{*} = 0.14$			$V_{cnt}^{*} = 0.17$		
		UD	FG–A	FG–B	UD	FG–A	FG–B	UD	FG–A	FG–B
300	1	0.4965	0.8081	0.4147	0.4397	0.7002	0.3760	0.3177	0.5180	0.2675
	2	0.4965	0.5689	0.4411	0.4397	0.5035	0.3891	0.3177	0.3616	0.2798
	3	0.4965	0.5282	0.4649	0.4397	0.4673	0.4094	0.3177	0.3355	0.2950
400	1	0.5830	0.9297	0.4965	0.5204	0.8079	0.4539	0.3723	0.5920	0.3204
	2	0.5830	0.6702	0.5177	0.5204	0.5976	0.4604	0.3723	0.4246	0.3276
	3	0.5830	0.6219	0.5446	0.5204	0.5545	0.4832	0.3723	0.3939	0.3448
500	1	0.7312	1.1271	0.6388	0.6596	0.9861	0.5898	0.4658	0.7114	0.4124
	2	0.7312	0.8444	0.6495	0.6596	0.7610	0.5842	0.4658	0.5329	0.4099
	3	0.7312	0.7833	0.6806	0.6596	0.7061	0.6100	0.4658	0.4944	0.4296
700	1	2.6592	3.6672	2.4815	2.4530	3.3410	2.3117	1.6856	2.2458	1.6041
	2	2.6592	3.2263	2.4125	2.4530	2.9974	2.2293	1.6856	2.0160	1.5126
	3	2.6592	3.0029	2.3927	2.4530	2.7941	2.1806	1.6856	1.8779	1.5019

Table 5 Effect of the geometric parameters the dimensionless central deflection of simply supported FG CNTRC plate ($V_{cnt}^{*} = 0.11,\ k = 1,\ T = 300\text{K},\ \text{N} = 1$)

Config.	b/a	***a/h***				
		5	**10**	**20**	**50**	**100**
UD	0.5	0.5321	0.2872	0.1991	0.1697	0.1653
	1	1.1620	0.4965	0.3062	0.2507	0.2427
	2	1.3338	0.5375	0.3258	0.2656	0.2569
	3	1.3552	0.5428	0.3285	0.2677	0.2590
FG–A	0.5	0.5847	0.3649	0.2959	0.2744	0.2713
	1	1.5252	0.8081	0.6089	0.5514	0.5431
	2	1.8817	0.9374	0.6944	0.6259	0.6161
	3	1.9354	0.9570	0.7077	0.6376	0.6276
FG–B	0.5	0.5083	0.2547	0.1574	0.1234	0.1182
	1	1.0778	0.4147	0.2216	0.1650	0.1568
	2	1.2241	0.4423	0.2318	0.1717	0.1631
	5	1.2410	0.4456	0.2332	0.1726	0.1639

Table 6 Effect of nonlocal and length scale parameters on the dimensionless central deflection $(V_{cnt}^{*} = 0.11,\ a = b,\ a/h = 10,\ N = 1)$

BCs.	λ	μ				
		0	0.5	1	1.5	2
SSSS	0	0.4147	0.4556	0.4966	0.5375	0.5784
	0.5	0.3774	0.4147	0.4520	0.4892	0.5265
	1	0.3463	0.3805	0.4147	0.4489	0.4831
	1.5	0.3200	0.3515	0.3831	0.4147	0.4463
	2	0.2973	0.3267	0.3560	0.3854	0.4147
CCCC	0	0.3699	0.4064	0.4430	0.4795	0.5160
	0.5	0.2924	0.3212	0.3501	0.3790	0.4078
	2	0.2417	0.2656	0.2894	0.3133	0.3371
	1.5	0.2060	0.2264	0.2467	0.2670	0.2874
	2	0.1795	0.1972	0.2149	0.2327	0.2504
CCSS	0	0.3015	0.3312	0.3610	0.3908	0.4205
	0.5	0.2424	0.2663	0.2902	0.3141	0.3381
	2	0.2027	0.2227	0.2427	0.2627	0.2827
	1.5	0.1741	0.1913	0.2085	0.2257	0.2428
	2	0.1526	0.1677	0.1827	0.1978	0.2129
CSCS	0	0.1241	0.1364	0.1486	0.1609	0.1731
	0.5	0.1022	0.1123	0.1224	0.1325	0.1426
	2	0.0869	0.0955	0.1040	0.1126	0.1212
	1.5	0.0756	0.0830	0.0905	0.0979	0.1054
	2	0.0669	0.0735	0.0801	0.0867	0.0933

Table 7 Effect of Winkler elastic foundation parameters of bending deflection of simply supported FG-B CNTRC plate $(V_{cnt}^{*} = 0.11,\ a = b,\ a/h = 10,\ k = 1, T = 300\text{K})$

κ	ξ	Sinusoidal	Reverse sinusoidal	Parabolic	Reverse parabolic
10	10	0.4113	0.4130	0.4129	0.4114
	10^2	0.3966	0.4130	0.4119	0.3976
	10^3	0.2923	0.4130	0.4026	0.2977
10^2	10	0.3966	0.3982	0.3981	0.3967
	10^2	0.3829	0.3982	0.3972	0.3839
	10^3	0.2848	0.3982	0.3885	0.2899
10^3	10	0.2923	0.2931	0.2931	0.2923
	10^2	0.2848	0.2931	0.2926	0.2853
	10^3	0.2267	0.2931	0.2879	0.2299

where

$$D_0 = \frac{E_p^0 h^3}{12\left(1-\upsilon_p{}^2\right)} \tag{46}$$

Here, E_p^0 is the polymer Young's modulus at the ambient temperature $(T = 300°K)$.

The dimensionless critical buckling loads:

$$\bar{N} = N_{cr}\frac{a^2}{D_0\pi^2} \tag{47}$$

The dimensionless frequency:

$$\bar{\omega} = \omega h\sqrt{\frac{\rho_p}{E_p^0}} \tag{48}$$

The foundation parameters:

$$k_w = \frac{a^2 b^2}{D_0}K_w \tag{49}$$

4.1 Bending analysis

In order to examine the response of CNTRC plate subjected to transverse sinusoidal loadings, Table 3 presents a comparative analysis of the dimensionless central deflections by considering the existed CNTs patterns in the literature (UD, FG X, FG O, FG V), and by examining the impact of CNTs volume fraction V_{cnt}^{*} and CNTs distribution patterns. It can be observed that the proposed

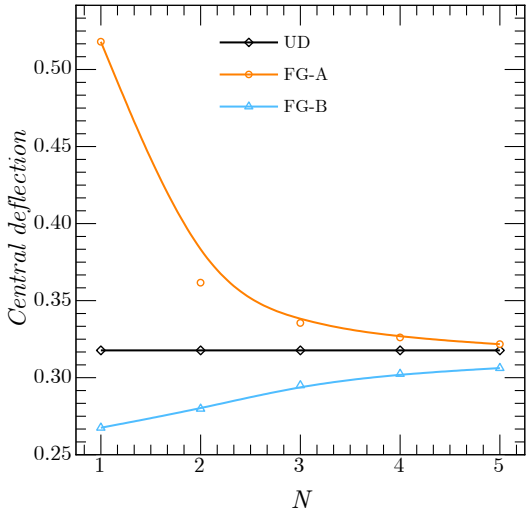

Fig. 3 Dimensionless central deflection versus material properties parameter N $(SSSS,\ V_{cnt}^{*} = 0.11,\ a = b,\ a/h = 10, T = 300\text{K},\ \mu = \lambda = 0)$

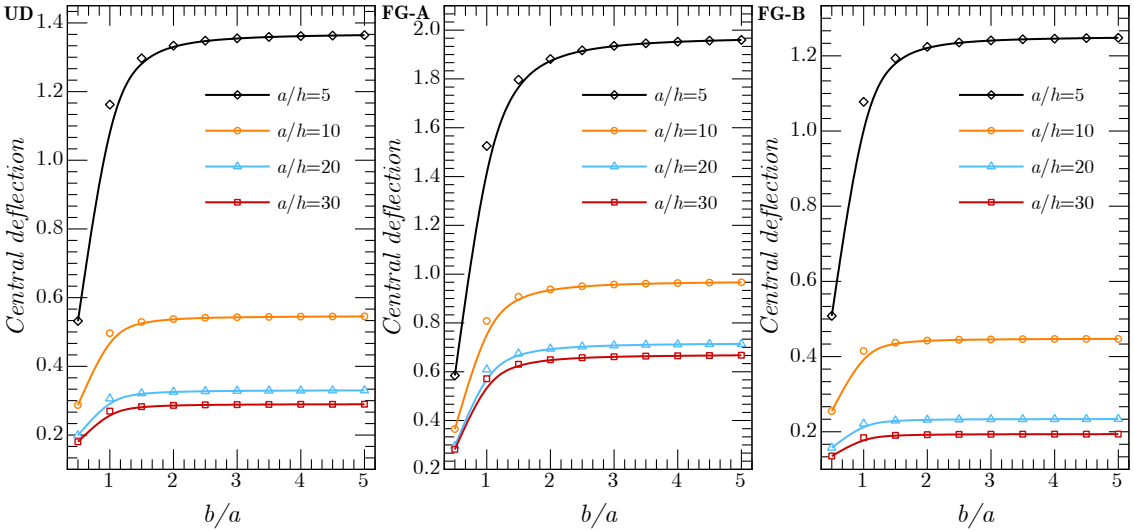

Fig. 4 Effect of the plate geometry on the dimensionless central deflection $(SSSS,\ V_{cnt}^{*} = 0.11,\ T = 300\text{K},\ N = 1, \mu = \lambda = 0)$

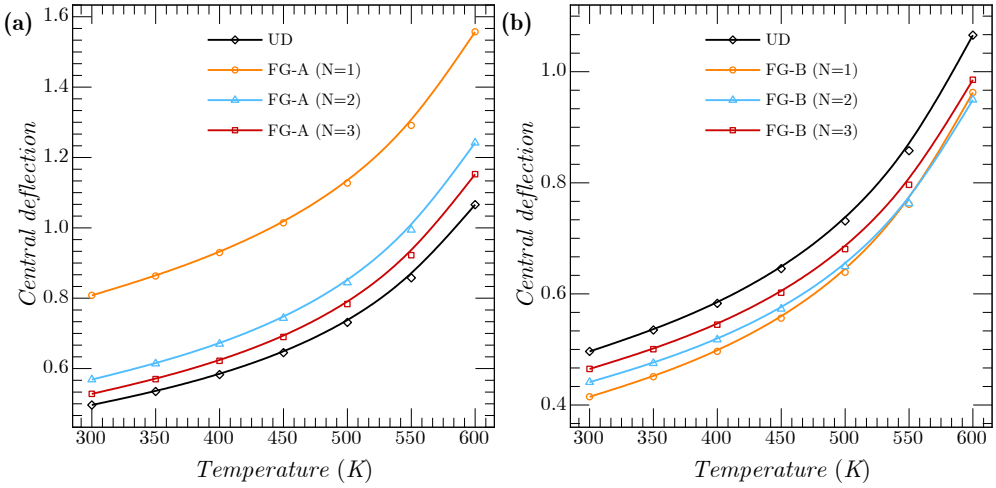

Fig. 5 Effect of temperature on the dimensionless central deflection $(SSSS,\ V_{cnt}^{*} = 0.11,\ a = b,\ a/h = 10,\ \mu = \lambda = 0)$

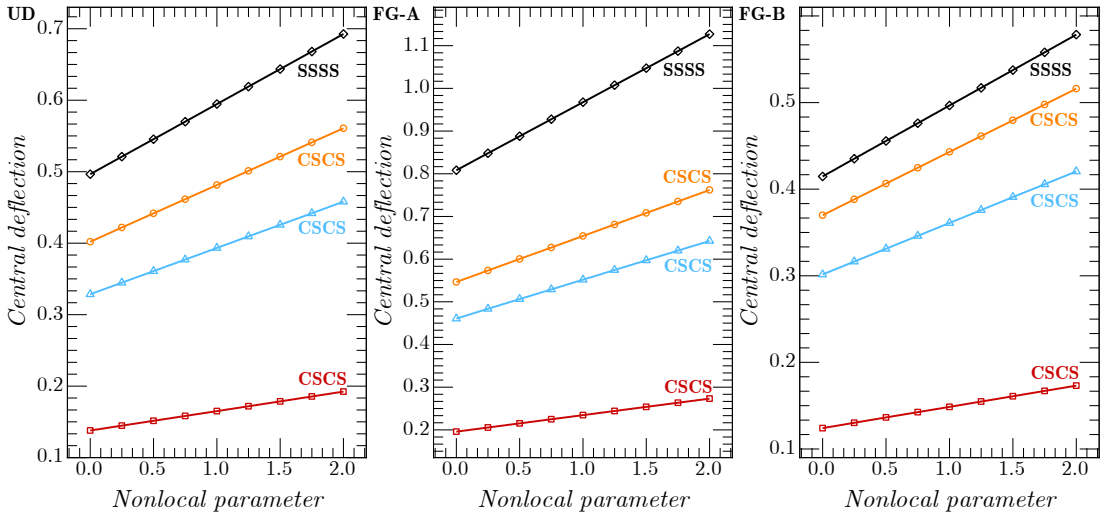

Fig. 6 Effect of nonlocal parameter on the dimensionless central deflection ($T = 300\text{K},\ V_{cnt}^{*} = 0.11,\ a = b,\ a/h = 10,\ \lambda = 0$)

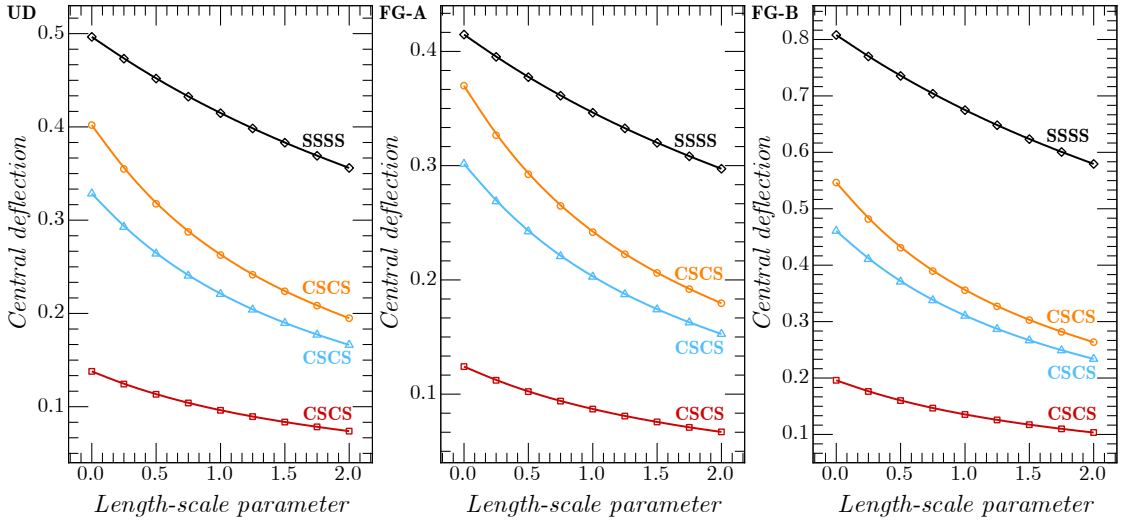

Fig. 7 Effect of length-scale parameter on the dimensionless central deflection ($T = 300\text{K},\ V_{cnt}^{*} = 0.11,\ a = b, a/h = 10,\ \mu = 0$)

pattern FG-B produce an excellent stiffness.

In the same Table, the results obtained by the present method and theory are compared with the analytical solution of Wattanasakulpong and Chaikittiratana (2013) using the third-order shear deformation theory (Reddy 1984) and the sinusoidal shear deformation theory (Touratier 1991). It can be observed that our results are absolutely identical to those generated by using the TSDT.

In Table 4, the impact of temperature, the homogeneity parameter *N*, volume fraction V_{cnt}^{*} and CNTs distribution patterns on the central deflection of the composite plates is illustrated. It is noticed that the mentioned parameters have a significant effect on the bending response.

The effect of the geometric parameters *b*/*a* and *a*/*h* on the dimensionless central deflection of simply supported FG CNTRC plate is illustrated in Fig. 5. The side-to-thickness ratio *a*/*h* is changed from 5 to 100, while the aspect ratio *b*/*a* is changed from 0.5 to 3. various CNTs distribution patterns are analysed. It is noted that dimensionless central deflections increase by the increase of the aspect ratio and by the decrease of the side-to-thickness ratio.

The influence of nonlocal and length scale parameters on the dimensionless central deflection of CNTRC nanoplates for various boundary conditions is illustrated in Fig. 6. The nonlocal and the length scale parameters are changed from 0 to 2.

Table 7 investigated the bending response of simply supported square FG-B CNTRC plates rested on different variable Winkler elastic foundations. It is noted that the increase of the foundation parameters κ and ξ leads to a decrement of the bending deflection.

The influence of the material properties parameter *N* is presented in Fig. 3. The increase of the parameter *N* leads to an increment in the deflection of the FG-B CNTRC plate, and a decrement in the deflection of the FG-B CNTRC plate. The UD distribution is unrelated to the parameter *N*, therefore, the deflection results are constant.

The effect of the geometry of the plate on the

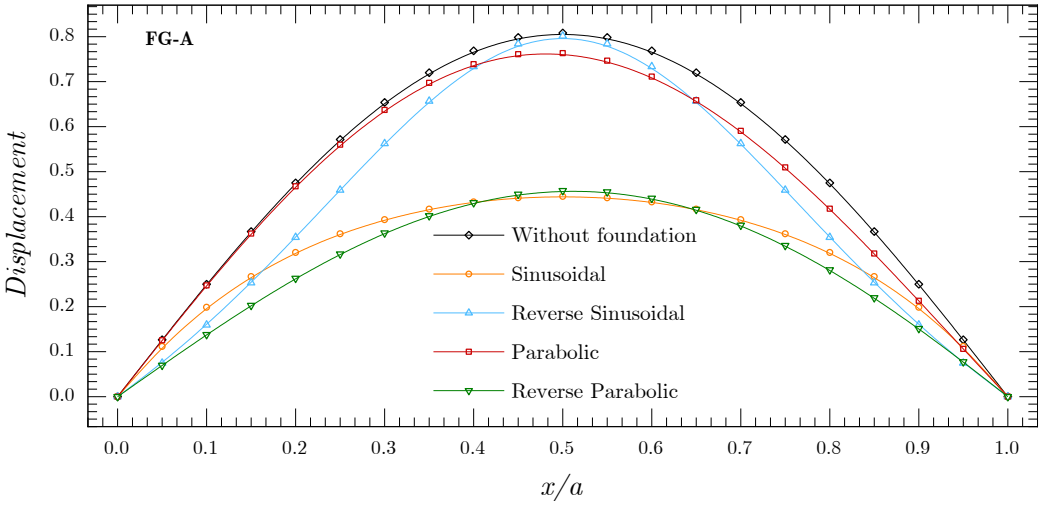

Fig. 8 Effect of the variable elastic foundation on the transverse displacement $(SSSS,\ T = 300\text{K},\ V_{cnt}^{*} = 0.11, a = b, a/h = 10, FG-A,\ K_1 = 10,\ K_2 = 1000,\ \mu = \lambda = 0)$

Table 8 Effect of the volume fraction, the CNTs distributions and boundary conditions on dimensionless critical buckling loads of CNTRC plates $(a = b,\ a/h = 10,\ T = 300\text{K})$

BCs.	$V_{cnt}^{*} = 0.11$			$V_{cnt}^{*} = 0.14$			$V_{cnt}^{*} = 0.17$		
	UD	FG–A	FG–B	UD	FG–A	FG–B	UD	FG–A	FG–B
Uniaxial compressive load									
SSSS	20.6579	12.6983	24.7465	23.3386	14.6693	27.2969	32.2849	19.9117	38.3567
CCCC	34.0809	25.3223	37.0169	36.8920	27.8940	39.5270	53.6697	40.7952	57.5767
CCSS	31.2822	22.4409	34.0611	33.9841	24.9616	36.3824	49.2313	36.1239	52.6578
CSCS	29.8112	21.1216	33.0960	32.5696	23.5940	35.5186	46.8622	33.7411	51.4174
Biaxial compressive load									
SSSS	10.3289	6.3491	12.3733	11.6693	7.3347	13.6485	16.1424	9.9559	19.1783
CCCC	17.0405	12.6611	18.5085	18.4460	13.9470	19.7635	26.8349	20.3976	28.7884
CCSS	17.8755	12.8234	19.4635	19.4195	14.2638	20.7899	28.1322	20.6422	30.0902
CSCS	14.9056	10.5608	16.5480	16.2848	11.7970	17.7593	23.4311	16.8706	25.7087

dimensionless central deflection of simply supported CNTRC plate is presented in Fig. 4. It is observed that the central deflection increases by the increase of the aspect ratio parameter *b*/*a* wherever the kind of the distribution is. for the values of aspect ratio *b*/*a* more than 2, the results are almost constant. In addition, the dimensionless central deflections increase when the thickness ratio parameter decreases.

The impact of temperature on the bending response of various types of simply supported CNTRC plates is examined in Fig. 5. It is noticeable that the augmentation of temperature reduces the CNTRC plate stiffness, and subsequently, the deflection of the plate increase, regardless of the CNTs distribution. It is clear from Fig. 5(b) that the FG-B CNTRC plate with N = 3 is the stiffer plate.

Fig. 6 plotted the central deflection of various CNTRC plates affected by the nonlocal parameter μ using various boundary conditions. The nonlocal parameter μ is changed from 0 to 2. It can be seen from this figure that the inclusion of nonlocal parameter reduces the plate stiffness, and therefore augment the central deflections.

Fig. 7 plotted the central deflection of various CNTRC plates affected by the length-scale parameter λ. Unlike the nonlocal parameter effect, it is observed that the dimensionless central deflection decreases by the increase of the length-scale parameter.

The effect of the variable elastic foundation on the transverse displacement of simply supported square FG-A CNTRC plate is shown in Fig. 8. To view the effect of the variable part of the foundation, the coefficient of the constant part of the foundation is fixed at $\kappa = 10$, whereas the second coefficient related to the variable part of the foundation is taken as $\xi = 1000$. From the plotted graphs, it is seen that the plates rested on the sinusoidal and the reverse parabolic foundations have fewer deflections than the other foundations.

4.2 Buckling analysis

Table 8 presents the dimensionless critical buckling load of various types of CNTRC plates subjected to uniaxial or biaxial compressive loadings. The influence of different

Table 9 Influence of temperature, length scale and nonlocal parameters on the dimensionless buckling load ($SSSS,\ V_{cnt}^{*}=0.11,\ a=b,\ a/h=10,\ FG-B$)

μ	λ	Temperature			
		300	400	500	700
0	0	12.3733	10.3378	8.0350	2.0686
	0.5	13.5944	11.3581	8.8280	2.2728
	1	14.8156	12.3784	9.6210	2.4769
	1.5	16.0368	13.3987	10.4140	2.6811
	2	17.2580	14.4190	11.2070	2.8853
0.5	0	11.2618	9.4091	7.3132	1.8828
	0.5	12.3733	10.3378	8.0350	2.0686
	1	13.4847	11.2664	8.7567	2.2544
	1.5	14.5962	12.1951	9.4785	2.4403
	2	15.7077	13.1237	10.2003	2.6261
1	0	10.3335	8.6336	6.7104	1.7276
	0.5	11.3534	9.4857	7.3727	1.8981
	1	12.3733	10.3378	8.0350	2.0686
	1.5	13.3931	11.1899	8.6973	2.2391
	2	14.4130	12.0420	9.3595	2.4096
1.5	0	9.5466	7.9761	6.1994	1.5960
	0.5	10.4888	8.7634	6.8113	1.7536
	1	11.4310	9.5506	7.4231	1.9111
	1.5	12.3733	10.3378	8.0350	2.0686
	2	13.3155	11.1250	8.6468	2.2261
2	0	8.8711	7.4117	5.7607	1.4831
	0.5	9.7466	8.1433	6.3293	1.6295
	1	10.6222	8.8748	6.8978	1.7759
	1.5	11.4977	9.6063	7.4664	1.9222
	2	12.3733	10.3378	8.0350	2.0686

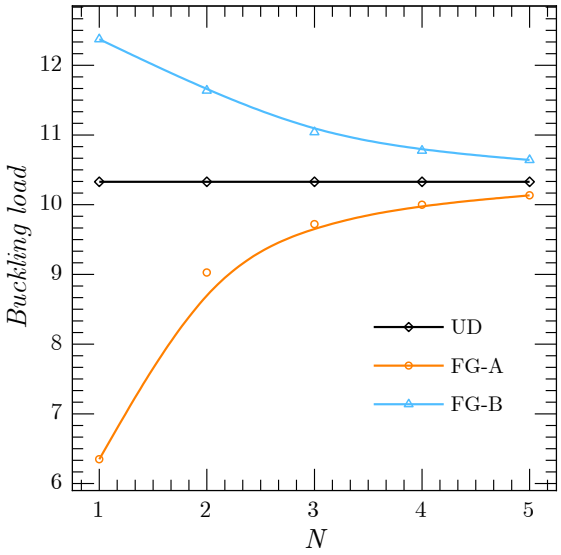

Fig. 9 Dimensionless critical buckling load versus material properties parameter N ($SSSS,\ T=300\text{K},\ V_{cnt}^{*}=0.11,\ a=b, a/h=10,\ \chi_1=-1, \chi_2=-1,\ \mu=\lambda=0$)

boundary conditions, CNTs volume fraction and CNTs distribution patterns is investigated.

In Table 9, the buckling response of FG-B CNTRC nanoplate influenced by biaxial compressive loads and thermal environment is investigated. The effect nonlocal and length scale parameters are included. it can be seen that the augmentation of temperature and nonlocal parameter λ decrease the critical buckling load, unlike the length scale parameter.

The influence of the material properties parameter N on the dimensionless critical buckling load of simply supported square CNTRC plates subjected to two in-plane compressive loads is plotted in Fig. 9. It observed that the increase of the parameter N leads to decrement in the critical buckling load of the FG-B CNTRC plate, and increment in in the buckling load of the FG-B CNTRC plate.

The influence of the thermal environment on the dimensionless critical buckling load of simply supported square CNTRC plate is illustrated in Fig 10. It can be noted that the critical buckling load was reduced to half when the temperature augment to 600K.

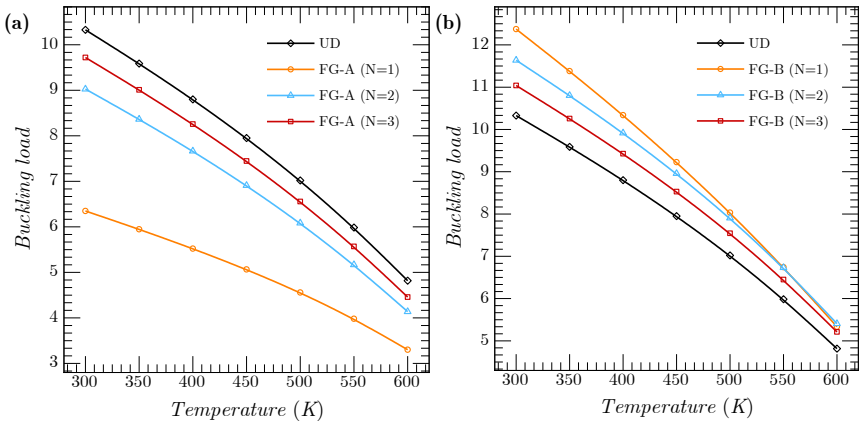

Fig. 10 Effect of temperature on the dimensionless critical buckling load ($SSSS$, $V_{cnt}^{*} = 0.11$, $a = b$, $a/h = 10$, $\chi_1 = \chi_2 = -1$, $\mu = \lambda = 0$)

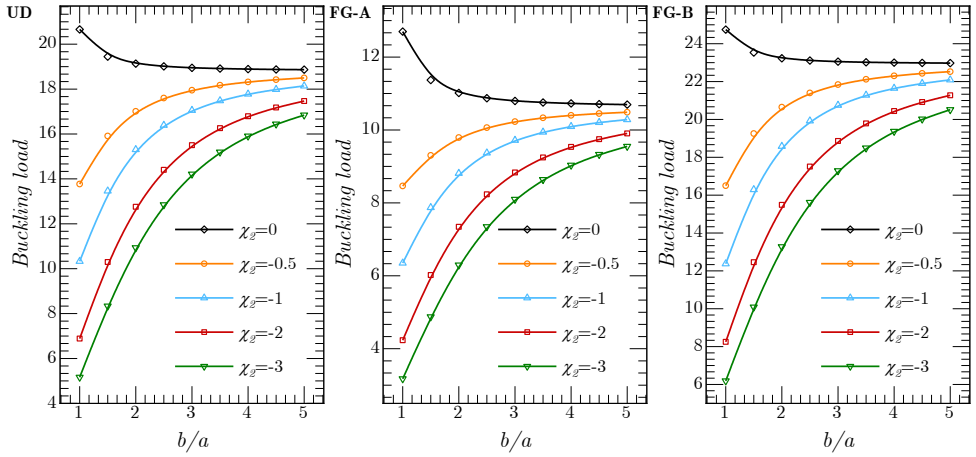

Fig. 11 Effect of the aspect ratio and the in-plane compressive loading intensity on the dimensionless critical buckling load ($SSSS$, $T = 300\text{K}$, $V_{cnt}^{*} = 0.11$, $a/h = 10$, $\chi_1 = -1$, $\mu = \lambda = 0$)

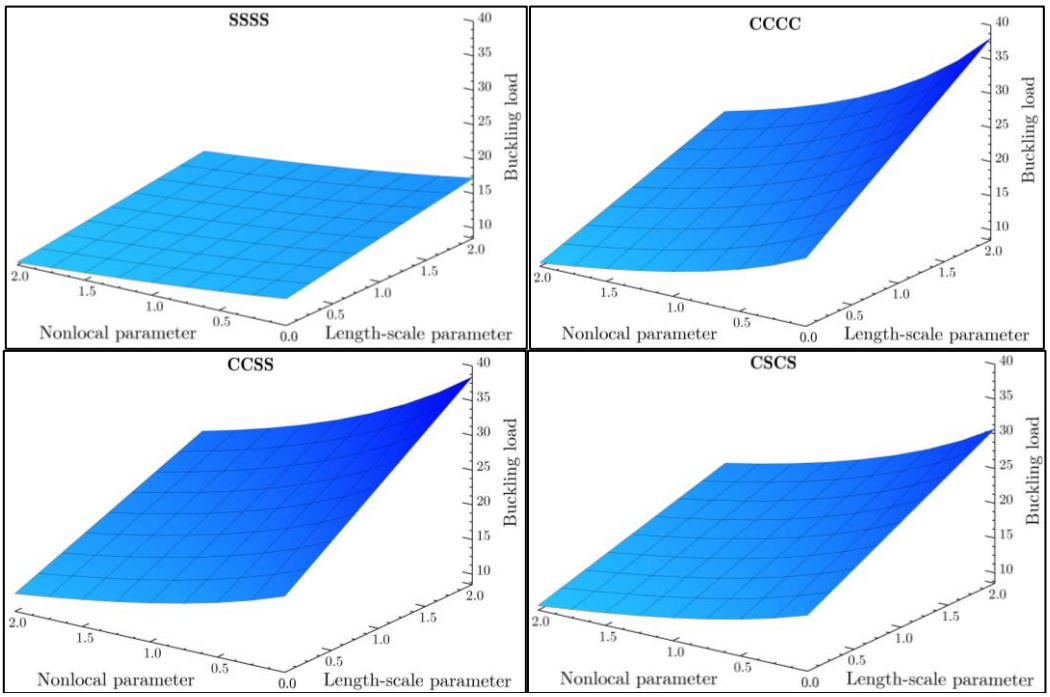

Fig. 12 Effect of the nonlocal parameter and the length scale parameter on the dimensionless critical buckling load ($T = 300\text{K}$, $V_{cnt}^{*} = 0.11$, $a = b$, $a/h = 10$, $FG - B$)

Table 9 Influence of temperature, length scale and nonlocal parameters on the dimensionless buckling load $(SSSS,\ V_{cnt}^{*}=0.11,\ a=b,\ a/h=10,\ FG-B)$

μ	λ	Temperature			
		300	400	500	700
0	0	0.1471	0.1345	0.1185	0.0601
	0.5	0.1542	0.1409	0.1242	0.0630
	1	0.1610	0.1471	0.1297	0.0658
	1.5	0.1675	0.1531	0.1349	0.0684
	2	0.1738	0.1588	0.1400	0.0710
0.5	0	0.1404	0.1283	0.1131	0.0573
	0.5	0.1471	0.1345	0.1185	0.0601
	1	0.1536	0.1404	0.1237	0.0627
	1.5	0.1598	0.1461	0.1287	0.0653
	2	0.1658	0.1515	0.1336	0.0677
1	0	0.1345	0.1229	0.1083	0.0549
	0.5	0.1409	0.1288	0.1135	0.0576
	1	0.1471	0.1345	0.1185	0.0601
	1.5	0.1531	0.1399	0.1233	0.0625
	2	0.1588	0.1451	0.1279	0.0649
1.5	0	0.1292	0.1181	0.1041	0.0528
	0.5	0.1355	0.1238	0.1091	0.0553
	1	0.1414	0.1292	0.1139	0.0578
	1.5	0.1471	0.1345	0.1185	0.0601
	2	0.1526	0.1395	0.1230	0.0623
2	0	0.1246	0.1139	0.1004	0.0509
	0.5	0.1306	0.1193	0.1052	0.0533
	1	0.1363	0.1246	0.1098	0.0557
	1.5	0.1418	0.1296	0.1143	0.0579
	2	0.1471	0.1345	0.1185	0.0601

Table 10 Effect of CNTs distribution and volume fraction on dimensionless frequencies of simply supported CNTRC plates $(a=b,\ a/h=10,\ T=300\mathrm{K})$

BCs.	$V_{cnt}^{*}=0.11$			$V_{cnt}^{*}=0.14$			$V_{cnt}^{*}=0.17$		
	UD	FG—A	FG—B	UD	FG—A	FG—B	UD	FG—A	FG—B
(1,1)	0.1345	0.1053	0.1471	0.1425	0.1129	0.1540	0.1670	0.1310	0.1820
(1,2)	0.3223	0.2731	0.3355	0.3348	0.2873	0.3454	0.4018	0.3443	0.4141
(2,2)	0.3402	0.2985	0.3524	0.3521	0.3112	0.3625	0.4244	0.3764	0.4371
(1,3)	0.5040	0.4367	0.5189	0.5226	0.4551	0.5353	0.6287	0.5541	0.6401
(2,3)	0.5153	0.4549	0.5292	0.5333	0.4723	0.5455	0.6429	0.5771	0.6542

The impact of the aspect ratio *b*/*a* and the in-plane compressive loading intensity on the dimensionless critical buckling load of simply supported square CNTRC plate is presented in Fig. 11. It is evident that the increase of compressive loading intensity leads to the decrement of critical buckling loads. In addition, the augmentation of the aspect ratio, increase the dimensionless critical buckling loads in the existence of the compressive loading in *y*-direction.

Figs. 12 plotted the impact of the nonlocal parameter and the length scale parameter on the dimensionless critical buckling load of FG-B CNTRC plate for various boundary conditions. From these figures, it can be found that the dimensionless critical buckling load reduces by increasing the length scale parameter and decreasing the nonlocal parameter.

4.3 Free Vibration analysis

Table 10 depicts the effect of CNTs distribution and volume

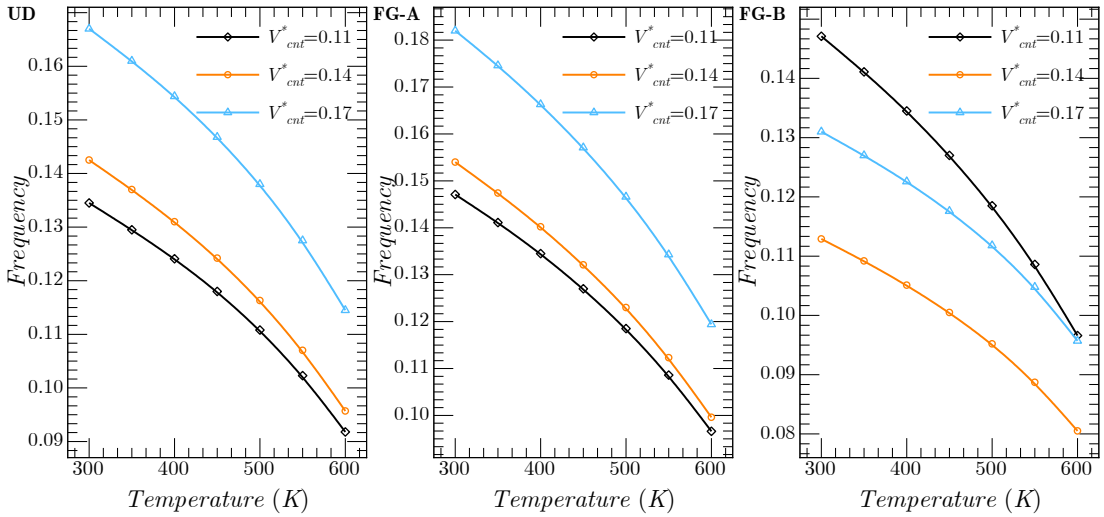

Fig. 13 Effect of the temperature and the CNTs volume fraction on the dimensionless critical buckling load $(SSSS, a = b,\ a/h = 10,\ \mu = \lambda = 0)$

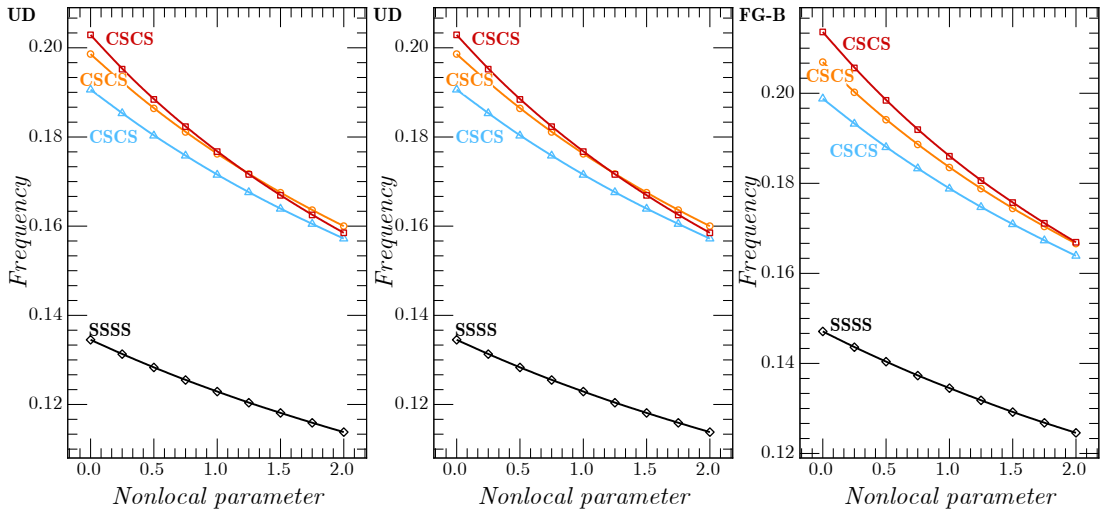

Fig. 14 Effect of nonlocal parameter on the dimensionless frequency $(T = 300\text{K},\ V^*_{cnt} = 0.11,\ a = b,\ a/h = 10,\ \lambda = 0)$

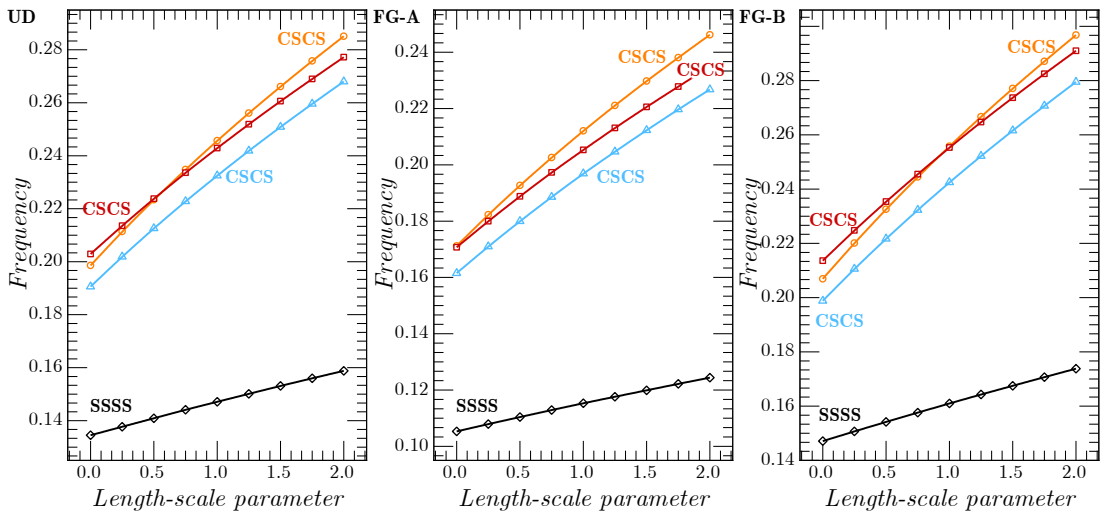

Fig. 15 Effect of length-scale parameter on the dimensionless frequency $(T = 300\text{K},\ V^*_{cnt} = 0.11,\ a = b,\ a/h = 10,\ \mu = 0)$

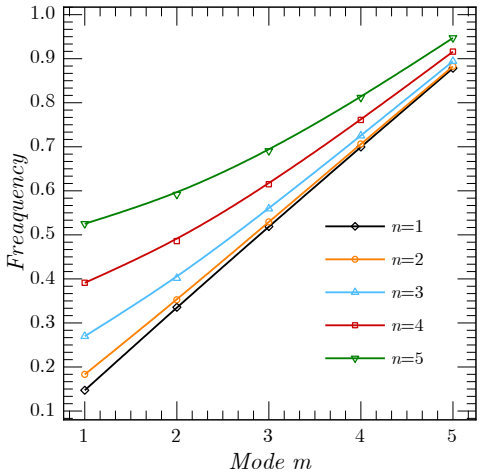

Fig. 16 Effect of mode numbers on the dimensionless frequency $(SSSS,\ T = 300\text{K},\ V_{cnt}^{*} = 0.11,\ a = b,\ a/h = 10,\ FG - B,\ \mu = \lambda = 0)$

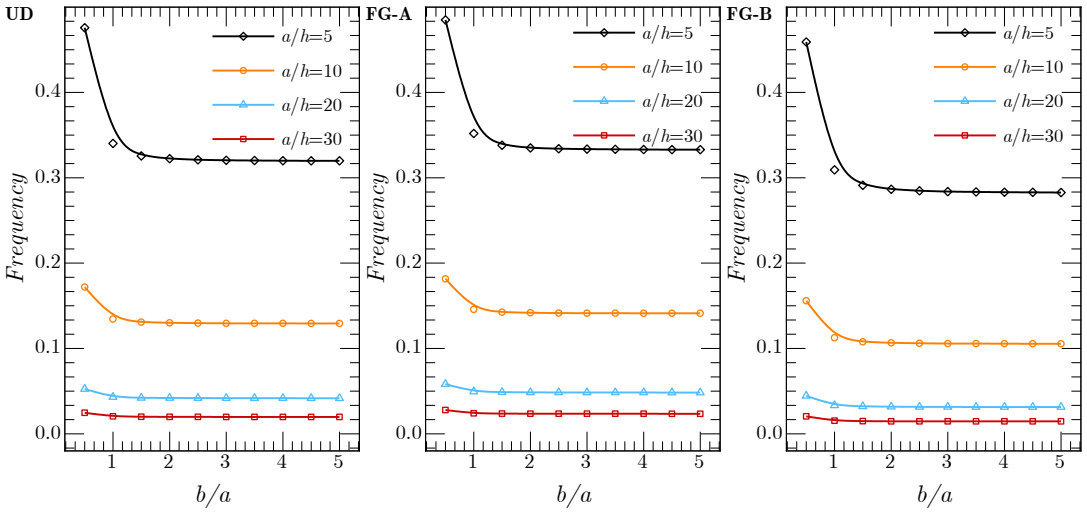

Fig. 17 Effect of the plate geometry on the dimensionless frequency $(SSSS,\ V_{cnt}^{*} = 0.11,\ T = 300\text{K},\ N = 1,\ \mu = \lambda = 0)$

fraction on dimensionless frequencies of CNTRC plates for various mode shape numbers *m* and *n*. It is clear and evident that the increase of mode number leads to an increment of frequencies.

The influence of temperature, length scale and nonlocal parameters on the dimensionless frequency of simply supported square FG-B CNTRC plate is examined in Table 11. The dimensionless frequency decrease by the increase of both temperature and nonlocal parameter.

The impact of temperature and CNTs volume fraction on simply supported square CNTRC plate is shown in Fig. 13. We can see that the stiffness of the plate has been improved by increasing CNTs volume fraction and decreasing temperature.

In Fig. 14, we plot the dimensionless frequency of CNTRC nanoplates with various boundary conditions influenced by the nonlocal parameter. As we obtained previously, the inclusion of the nonlocal parameter reduces the plate stiffness, therefore the frequencies decrease. The opposite effect is obtained in Fig 15 by including the length scale parameter.

The effect of mode numbers on the dimensionless frequency of simply supported square FG-B CNTRC plates is carried out in Fig. 16. The augmentation of the modes n and m increase the dimensionless frequency.

The impact of the geometry parameters *b*/*a* and *a*/*h* on the dimensionless frequency of simply supported CNTRC plate is plotted in Fig. 17. From this figure, the dimensionless frequency decreases by the increase of the aspect ratio parameter *b*/*a* wherever the kind of the distribution is for for the values of aspect ratio *b/a* more than 2, the results are almost constant. In addition, the dimensionless central deflections decrease when the thickness ratio parameter decreases.

5. Conclusions

In the present article, a new quasi-3D nonlocal higher-order shear deformation theory is performed to study the mechanical behaviour of new types of CNTRC nanoplates. Four variables are employed here to define the field of the

displacement. Two new forms of CNTs reinforcement distribution are proposed based on cosine functions. Based on Galerkin method, analytical approach is developed to derive the governing equilibrium equations of the CNTRC nanoplate to cover different boundary conditions. A novel two-dimensional variable Winkler elastic foundation is suggested in this study. The accuracy of the new solution and theory is verified by comparing the results obtained with the other analytical solutions and theories. Numerical results are presented and discussed in detail of bending, buckling and vibration of CNTRC nanoplates resting on the variable Winkler foundation with various Boundary conditions. The main conclusions and observations can be summarized as:

• The proposed theory is in close agreement with shear deformation theory of Reddy.

• The stiffness of the CNTRC plate has been improved by using FG-B CNTs distribution, therefore increasing the critical buckling loads and frequencies and decreasing the bending deflections.

• The inhomogeneity parameter has a significant effect to improve the FG-A CNTRC plate stiffness, and an inverse effect is remarked for the FG-B distribution.

• The integration of nonlocal parameter reduces the stiffness, therefore augments the transverse displacements and decrease the frequencies and the buckling loads, while the opposite is produced when increasing the length-scale parameter.

• The inclusion of a thermal environment reduces the stiffness of the plate, the bending deflections increase and the frequencies and buckling loads decrease.

Acknowledgments

The Deanship of Scientific Research (DSR) at King Abdulaziz University, Jeddah, Saudi Arabia has funded this project, under grant No. (FP-129-43).

References

Abdelrahman, A.A., Esen, I., Özarpa, C. and Eltaher, M.A. (2021), "Dynamics of perforated nanobeams subject to moving mass using the nonlocal strain gradient theory", *Appl. Math. Modell.*, **96**, 215-235. https://doi.org/10.1016/j.apm.2021.03.008.

Abo-Bakr, R.M., Eltaher, M.A. and Attia, M.A. (2020), "Pull-in and freestanding instability of actuated functionally graded nanobeams including surface and stiffening effects", *Eng. Comput.*, 1-22. https://doi.org/10.1007/s00366-020-01146-0.

Abualnour, M., Houari, M.S.A., Tounsi, A. and Mahmoud, S.R. (2018), "A novel quasi-3D trigonometric plate theory for free vibration analysis of advanced composite plates", *Compos. Struct.*, **184**, 688-697. http://doi.org/10.1016/j.compstruct.2017.10.047.

Akbaş, Ş.D., Fageehi, Y.A., Assie, A.E. and Eltaher, M.A. (2020), "Dynamic analysis of viscoelastic functionally graded porous thick beams under pulse load", *Eng. Comput.*, 1-13. https://doi.org/10.1007/s00366-020-01070-3.

Alazwari, M.A., Daikh, A.A., Houari, M.S.A., Tounsi, A. and Eltaher, M.A. (2021), "On static buckling of multilayered carbon nanotubes reinforced composite nanobeams supported on non-linear elastic foundations", *Steel Compos. Struct.*, **40**(3), 389-404. http://doi.org/10.12989/scs.2021.40.3.389.

Alibeigloo, A. (2018), "Coupled thermoelasticity analysis of carbon nano tube reinforced composite rectangular plate subjected to thermal shock", *Compos. Part B Eng.*, **153**, 445-455. https://doi.org/10.1016/j.compositesb.2018.09.003.

Amiri, A., Mohammadimehr, M. and Anvari, M. (2020), "Stress and buckling analysis of a thick-walled micro sandwich panel with a flexible foam core and carbon nanotube reinforced composite (CNTRC) face sheets", *Appl. Math. Mech.*, **41**(7), 1027-1038. https://doi.org/10.1007/s10483-020-2627-7.

Bekhadda, A., Cheikh, A., Bensaid, I., Hadjoui, A. and Daikh, A.A. (2019), "A novel first order refined shear-deformation beam theory for vibration and buckling analysis of continuously graded beams", *Adv. Aircr. Spacecr. Sci.*, **6**(3), 189-206. https://doi.org/10.12989/aas.2019.6.3.189.

Ghorbanpour-Arani, A., Kolahdouzan, F. and Abdollahian, M. (2018), "Nonlocal buckling of embedded magnetoelectroelastic sandwich nanoplate using refined zigzag theory", *Appl. Math. Mech.*, **39**(4), 529-546. https://doi.org/10.1007/s10483-018-2319-8.

Arshid, E., Arshid, H., Amir, S. and Mousavi, S.B. (2021), "Free vibration and buckling analyses of FG porous sandwich curved microbeams in thermal environment under magnetic field based on modified couple stress theory", *Arch. Civil Mech. Eng.*, **21**(1), 1-23. https://doi.org/10.1007/s43452-020-00150-x.

Belarbi, O.M., Houari, M.S.A., HIRANE, H. and Daikh, A.A. (2020), "An efficient nonlocal finite element model for the bending and buckling analysis of functionally graded nanobeams using a novel parabolic shear deformation theory", *Compos. Struct.*, **264**, 113712. https://doi.org/10.1016/j.compstruct.2021.113712.

Bensaid, I. (2017), "A refined nonlocal hyperbolic shear deformation beam model for bending and dynamic analysis of nanoscale beams", *Adv. Nano Res.*, **5**(2), 113-126. http://doi.org/10.12989/anr.2017.5.2.113.

Bouazza, M., Kenouza, Y., Benseddiq, N. and Zenkour, A. M. (2017), "A two-variable simplified nth-higher-order theory for free vibration behavior of laminated plates", *Compos. Struct.*, **182**, 533-541. http://doi.org/10.1016/j.compstruct.2017.09.041.

Daikh, A.A. (2019), "Temperature dependent vibration analysis of functionally graded sandwich plates resting on Winkler/ Pasternak/Kerr foundation", *Mater. Res. Express.*, **6**, 065702. https://doi.org/10.1088/2053-1591/ab097b.

Daikh, A.A., Drai, A., Houari M.S.A. and Mohamed A. Eltaher. (2020a), "Static analysis of multilayer nonlocal strain gradient nanobeam reinforced by carbon nanotubes", *Steel Compos. Struct.*, **36**(6), 643-656. https://doi.org/10.12989/scs.2020.36.6.643.

Daikh, A.A., Bachiri, A., Houari, M.S.A. and Tounsi. (2020b), "Size dependent free vibration and buckling of multilayered carbon nanotubes reinforced composite nanoplates in thermal environment", *Mech. Based Des. Struct.*, 1-29. https://doi.org/10.1080/15397734.2020.1752232.

Daikh, A.A., Houari, M.S.A. and Eltaher. M.A. (2020c), "A novel nonlocal strain gradient Quasi-3D bending analysis of sigmoid functionally graded sandwich nanoplates", *Compos. Struct.*, 113347. https://doi.org/10.1016/j.compstruct.2020.113347.

Daikh, A.A., Houari, M.S.A. and Eltaher, M.A. (2021a), "A novel nonlocal strain gradient Quasi-3D bending analysis of sigmoid functionally graded sandwich nanoplates", *Compos. Struct.*, **262**, 113347. https://doi.org/10.1016/j.compstruct.2020.113347.

Daikh, A.A., Houari, M.S.A., Belarbi, M.O., Chakraverty, S. and Eltaher, M.A. (2021b), "Analysis of axially temperature-dependent functionally graded carbon nanotube reinforced composite plates", *Eng. Comput.*, 1-22. https://doi.org/10.1007/s00366-021-01413-8.

Daikh, A.A., Houari, M.S.A., Karami, B., Eltaher, M.A., Dimitri,

R. and Tornabene, F. (2021c), "Buckling analysis of CNTRC curved sandwich nanobeams in thermal environment", *Appl. Sci.*, **11**(7), 3250. https://doi.org/10.3390/app11073250.

Daikh, A.A., Houari, M.S.A., Belarbi, M.O., Mohamed, S.A. and Eltaher, M.A. (2021d), "Static and dynamic stability responses of multilayer functionally graded carbon nanotubes reinforced composite nanoplates via quasi 3D nonlocal strain gradient theory", *Defence Technol.*, In Press. https://doi.org/10.1016/j.dt.2021.09.011.

Daikh, A.A., Houari, M.S.A., Belarbi, M.O. Chakraverty, S. and Eltaher, M.A. (2021e), "Analysis of axially temperature-dependent functionally graded carbon nanotube reinforced composite plates", *Eng. Comput.*, 1-22. https://doi.org/10.1007/s00366-021-01413-8.

Ebrahimi, F. and Barati, A.F. (2016), "Analytical solution for nonlocal buckling characteristics of higher-order inhomogeneous nanosize beams embedded in elastic medium", *Adv. Nano Res.*, **4**(3), 229-249. http://doi.org/10.12989/anr.2016.4.3.229.

Ehyaei, J., Akbarshahi, A., and Shafiei, N. (2017), "Influence of porosity and axial preload on vibration behavior of rotating FG nanobeam", *Adv. Nano Res.*, **5**(2), 141-169. http://doi.org/10.12989/anr.2017.5.2.141.

Eltaher, M.A., El-Borgi, S. and Reddy, J.N. (2016a), "Nonlinear analysis of size-dependent and material-dependent nonlocal CNTs", *Compos. Struct.*, **153**, 902-913. https://doi.org/10.1016/j.compstruct.2016.07.013.

Eltaher, M.A., Khater, M.E., Park, S., Abdel-Rahman, E. and Yavuz M. (2016b), "On the static stability of nonlocal nanobeams using higher-order beam theories", *Adv. Nano Res.*, **4**(1), 51-64. http://doi.org/10.12989/anr.2016.4.1.051.

Eltaher, M.A., Agwa, M. and Kabeel, A. (2018), "Vibration analysis of material size dependent CNTs using energy equivalent model", *J. Appl. Computat. Mech.*, **4**(2), 75-86. https://doi.org/10.1016/j.compositesb.2018.09.003

Eltaher, M.A. and Mohamed, N. (2020), "Nonlinear stability and vibration of imperfect CNTs by doublet mechanics", *Appl. Math. Computat.*, **382**, 125311. https://doi.org/10.1016/j.amc.2020.125311.

Eltaher, M.A., Abdelrahman, A.A. and Esen, I. (2021), "Dynamic analysis of nanoscale Timoshenko CNTs based on doublet mechanics under moving load", *Eur. Phys. J. Plus*, **136**(7), 1-21. https://doi.org/10.1140/epjp/s13360-021-01682-8.

Eringen, A.C. (1972), "Nonlocal polar elastic continua", *Int. J. Eng. Sci.*, **10**(1), 1-16. https://doi.org/10.1016/0020-7225(72)90070-5.

Eringen, A.C. (1983), "On differential equations of nonlocal elasticity and solutions of screw dislocation and surface waves", *J. Appl. Phys.*, **54**(9), 4703-10. https://doi.org/10.1063/1.332803.

Esen, I., Abdelrhmaan, A.A. and Eltaher, M.A. (2021a), "Free vibration and buckling stability of FG nanobeams exposed to magnetic and thermal fields", *Eng. Comput.*, 1-20. https://doi.org/10.1007/s00366-021-01389-5.

Esen, I., Daikh, A.A. and Eltaher, M.A. (2021b), "Dynamic response of nonlocal strain gradient FG nanobeam reinforced by carbon nanotubes under moving point load", *Eur. Phys. J. Plus*, **136**(4), 1-22. https://doi.org/10.1140/epjp/s13360-021-01419-7.

Esen, I., Abdelrahman, A.A. and Eltaher, M.A. (2021), "On vibration of sigmoid/symmetric functionally graded nonlocal strain gradient nanobeams under moving load", *Int. J. Mech. Mater. Des.*, 1-22. https://doi.org/10.1007/s10999-021-09555-9.

Garg, A., Chalak, H.D., Belarbi, M.O., Zenkour, A.M. and Sahoo, R. (2021), "Estimation of carbon nanotubes and their applications as reinforcing composite materials–an engineering review", *Compos. Struct.*, 114234. https://doi.org/10.1016/j.compstruct.2021.114234.

Ghassabi, M., Zarastvand, M.R. and Talebitooti, R. (2020), "Investigation of state vector computational solution on modeling of wave propagation through functionally graded nanocomposite doubly curved thick structures", *Eng. Comput.*, **36**(4), 1417-1433. https://doi.org/10.1007/s00366-019-00773-6.

Ghobadi, A., Beni, Y.T. and Żur, K.K. (2021), "Porosity distribution effect on stress, electric field and nonlinear vibration of functionally graded nanostructures with direct and inverse flexoelectric phenomenon", *Compos. Struct.*, **259**, 113220. https://doi.org/10.1016/j.compstruct.2020.113220.

Gholami, R. and Ansari, R. (2018), "The effect of initial geometric imperfection on the nonlinear resonance of functionally graded carbon nanotube-reinforced composite rectangular plates", *Appl. Math. Mech.*, **39**(9), 1219-1238. https://doi.org/10.1007/s10483-018-2367-9.

Han, Y., and Elliott, J. (2007), "Molecular dynamics simulations of the elastic properties of polymer/carbon nanotube composites", *Computat. Mater. Sci.*, **39**(2), 315-323. https://doi.org/10.1016/j.commatsci.2006.06.011.

Hamed, M.A., Mohamed, S.A. and Eltaher, M.A. (2020), "Buckling analysis of sandwich beam rested on elastic foundation and subjected to varying axial in-plane loads", *Steel Compos. Struct.*, **34**(1), 75-89. https://doi.org/10.12989/scs.2020.34.1.075.

Hussain, M., Naeem, M.N. and Tounsi, A. (2020a), "Response of orthotropic Kelvin modeling for single-walled carbon nanotubes: Frequency analysis", *Adv. Nano Res.*, **8**(3), 229-244. https://doi.org/10.12989/anr.2020.8.3.229.

Hussain, M., Naeem, M.N., Asghar, S. and Tounsi, A. (2020b), "Theoretical impact of Kelvin's theory for vibration of double walled carbon nanotubes", *Adv. Nano Res.*, **8**(4), 307-322. https://doi.org/10.12989/anr.2020.8.4.307.

Karami, B., Shahsavari, D. and Janghorban, M. (2018), "A comprehensive analytical study on functionally graded carbon nanotube-reinforced composite plates", *Aerosp. Sci. Technol.*, **82**, 499-512. https://doi.org/10.1016/j.ast.2018.10.001.

Kolahdouzan, F., Mosayyebi, M., Ghasemi, F.A., Kolahchi, R. and Panah, S.R.M. (2020), "Free vibration and buckling analysis of elastically restrained FG-CNTRC sandwich annular nano-plates", *Adv. Nano Res.*, **9**(4), 237-250. http://doi.org/10.12989/anr.2020.9.4.237.

Li, X., Song, M., Yang, J. and Kitipornchai, S. (2019), "Primary and secondary resonances of functionally graded graphene platelet-reinforced nanocomposite beams", *Nonlinear Dynam.*, **95**(3), 1807-1826. https://doi.org/10.1007/s11071-018-4660-9.

Li, M., Soares, C.G. and Yan, R. (2021), "Free vibration analysis of FGM plates on Winkler/Pasternak/Kerr foundation by using a simple quasi-3D HSDT", *Compos. Struct.*, **264**, 113643. https://doi.org/10.1016/j.compstruct.2021.113643.

Lim, C.W., Zhang, G. and Reddy, J.N. (2015), "A higher-order nonlocal elasticity and strain gradient theory and its applications in wave propagation", *J. Mech. Phys. Solid*, **78**, 298-313. https://doi.org/10.1016/j.jmps.2015.02.001.

Melaibari, A., Abo-bakr, R.M., Mohamed, S.A. and Eltaher, M.A. (2020), "Static stability of higher order functionally graded beam under variable axial load", *Alexandria Eng. J.*, **59**(3), 1661-1675. https://doi.org/10.1016/j.aej.2020.04.012.

Qaderi, S. and Ebrahimi, F. (2020), "Vibration analysis of polymer composite plates reinforced with graphene platelets resting on two-parameter viscoelastic foundation", *Eng. Comput.*, 1-17. https://doi.org/10.1007/s00366-020-01066-z.

Reddy, J.N. (1984), "A simple higher-order theory for laminated composite plates", *J. Appl. Mech.*, **51**, 745-752. https://doi.org/10.1115/1.3167719.

Sahmani, S., Safaei, B. and Aldakheel, F. (2021), "Surface elastic-based nonlinear bending analysis of functionally graded nanoplates with variable thickness", *Eur. Phys. J. Plus*, **136**(6), 1-28. https://doi.org/10.1140/epjp/s13360-021-01667-7.

Sari, M.S., Ghaffari, S., Ceballes, S. and Abdelkefi, A. (2020), "Buckling response of functionally graded nanoplates under combined thermal and mechanical loadings", *J. Nanopart. Res.*, **22**(4), 1-21. https://doi.org/10.1007/s11051-020-04815-9.

Selim, B.A., Liu, Z. and Liew, K.M. (2019), "Active vibration control of functionally graded graphene nanoplatelets reinforced composite plates integrated with piezoelectric layers", *Thin Walled Struct.*, **145**, 106372. https://doi.org/10.1016/j.tws.2019.106372.

Shaban, M. and Mazaheri, H. (2021), "Bending analysis of five-layer curved functionally graded sandwich panel in magnetic field: closed-form solution", *Appl. Math. Mech.*, **42**(2), 251-274. https://doi.org/10.1007/s10483-021-2675-7.

Shakouri, M. and Mohseni, A. (2020), "Buckling analysis of rectangular sandwich plates with functionally graded graphene-reinforced face layers", *J. Brazil. Soc. Mech. Sci. Eng.*, **42**(10), 1-11. https://doi.org/10.1007/s40430-020-02620-y.

Shen, H.S. (2009), "Nonlinear bending of functionally graded carbon nanotube-reinforced composite plates in thermal environments", *Compos. Struct.*, **91**(1), 9-19. https://doi.org/10.1016/j.compstruct.2009.04.026.

Shojaee, M., Setoodeh, A.R. and Malekzadeh, P. (2017), "Vibration of functionally graded CNTs-reinforced skewed cylindrical panels using a transformed differential quadrature method", *Acta Mech.*, **228**(7), 2691-2711. https://doi.org/10.1007/s00707-017-1846-z.

Singh, P.P. and Azam, M.S. (2021), "Size dependent vibration of embedded functionally graded nanoplate in hygrothermal environment by Rayleigh-Ritz method", *Adv. Nano Res.*, **10**(1), 25-42. https://doi.org/10.12989/anr.2021.10.1.025.

Thai, C.H., Ferreira, A.J.M., Nguyen-Xuan, H., Nguyen, L.B. and Phung-Van, P. (2021), "A nonlocal strain gradient analysis of laminated composites and sandwich nanoplates using meshfree approach", *Eng. Comput.*, 1-17. https://doi.org/10.1007/s00366-021-01501-9.

Thai, H.T., Nguyen, T.K., Vo, T.P., Lee, J. (2014), "Analysis of functionally graded sandwich plates using a new first-order shear deformation theory", *Eur. J. Mech. A Solid*, **45**, 211-25. https://doi.org/10.1016/j.euromechsol.2013.12.008.

Touloukian, Y.S. (1967), *Thermophysical Properties of High Temperature Solid Materials*, MacMillan, London, U.K.

Touratier, M. (1991), "An efficient standard plate theory", *Int. J. Eng. Sci.*, **29**(8), 901-916. https://doi.org/10.1016/0020-7225(91)90165-Y.

Van Vinh, P. and Huy, L.Q. (2021), "Finite element analysis of functionally graded sandwich plates with porosity via a new hyperbolic shear deformation theory", *Defence Technol.*, In Press. https://doi.org/10.1016/j.dt.2021.03.006.

Wattanasakulpong, N., Chaikittiratana, A. (2015, "Exact solutions for static and dynamic analyses of carbon nanotube-reinforced composite plates with Pasternak elastic foundation", *Appl. Math. Modell.*, **39**, 5459-5472. https://doi.org/10.1016/j.apm.2014.12.058.

Yayli, M.Ö. (2015a), "Buckling analysis of a rotationally restrained single walled carbon nanotubes", *Acta Physica Pol. A*, **127**(3), 678-683. https://doi.org/10.12693/APhysPolA.127.678.

Yayli, M.Ö. (2015b), "Stability analysis of gradient elastic microbeams with arbitrary boundary conditions", *J. Mech. Sci. Technol.*, **29**, 3373-3380. https://doi.org/10.1007/s12206-015-0735-4.

Yayli, M.Ö. (2016), "An efficient solution method for the longitudinal vibration of nanorods with arbitrary boundary conditions via a hardening nonlocal approach", *J. Vib. Control*, **24**(11), 2230-2246. https://doi.org/10.1177/1077546316684042.

Yayli, M.Ö. (2018a), "On the torsional vibrations of restrained nanotubes embedded in an elastic medium", *J. Brazil. Soc. Mech. Sci. Eng.*, **40**, 419. https://doi.org/10.1007/s40430-018-1346-7.

Yayli, M.Ö. (2018b), "Torsional vibrations of restrained nanotubes using modified couple stress theory", *Microsyst. Technol.*, **24**(8), 3425-3435. https://doi.org/10.1007/s00542-018-3735-3.

Yayli, M.Ö. (2018c), "Torsional vibration analysis of nanorods with elastic torsional restraints using non-local elasticity theory", *Micro Nano Lett.*, **13**(5), 595-599. https://doi.org/10.1049/mnl.2017.0751.

Yayli, M.Ö. (2019), "Effects of rotational restraints on the thermal buckling of carbon nanotube", *Micro Nano Lett.*, **14**(2), 158-162. https://doi.org/10.1049/mnl.2018.5428.

Zaoui, F.Z., Ouinas, D. and Tounsi, A. (2019), "New 2D and quasi-3D shear deformation theories for free vibration of functionally graded plates on elastic foundations", *Compos. Part B Eng.*, **159**, 231-247. https://doi.org/10.1016/j.compositesb.2018.09.051.

Zheng, J., Zhang, C., Musharavati, F., Khan, A. and Sebaey, T.A. (2021), "Thermo-mechanical buckling analysis of FG-GNPs reinforced composites sandwich microplates using a trigonometric four-variable shear deformation theory", *Case Stud. Therm. Eng.*, 101120. https://doi.org/10.1016/j.csite.2021.101120.

CC